Functionally distinct resident macrophage subsets differentially shape responses to infection in the bladder

Livia Lacerda Mariano, Matthieu Rousseau, Hugo Varet, Rachel Legendre,
Rebecca Gentek, Javier Saenz Coronilla, Marc Bajenoff, Elisa Gomez
Perdiguero, Molly A Ingersoll

IMMUNOLOGY

Functionally distinct resident macrophage subsets differentially shape responses to infection in the bladder

Livia Lacerda Mariano[1,2], Matthieu Rousseau[1,2], Hugo Varet[3,4], Rachel Legendre[3,4], Rebecca Gentek[5]*, Javier Saenz Coronilla[6], Marc Bajenoff[5], Elisa Gomez Perdiguero[6], Molly A. Ingersoll[1,2†]

Resident macrophages are abundant in the bladder, playing key roles in immunity to uropathogens. Yet, whether they are heterogeneous, where they come from, and how they respond to infection remain largely unknown. We identified two macrophage subsets in mouse bladders, MacM in muscle and MacL in the lamina propria, each with distinct protein expression and transcriptomes. Using a urinary tract infection model, we validated our transcriptomic analyses, finding that MacM macrophages phagocytosed more bacteria and polarized to an anti-inflammatory profile, whereas MacL macrophages died rapidly during infection. During resolution, monocyte-derived cells contributed to tissue-resident macrophage pools and both subsets acquired transcriptional profiles distinct from naïve macrophages. Macrophage depletion resulted in the induction of a type 1–biased immune response to a second urinary tract infection, improving bacterial clearance. Our study uncovers the biology of resident macrophages and their responses to an exceedingly common infection in a largely overlooked organ, the bladder.

INTRODUCTION

Tissue-resident macrophages regulate immunity and are pivotal for development, homeostasis, and repair (1). Major research efforts have uncovered roles for tissue-resident macrophages during infection, insult, and repair. However, in many cases, these studies disproportionately focus on certain organs in animals while disregarding tissue macrophages in other locations (2). Because function in macrophages is shaped by their tissue of residence and the local environment, specific phenotypes may not be universally applicable to all tissues (3). Notably, the bladder has generally been overlooked in macrophage studies; consequently, the function, origin, and renewal of bladder-resident macrophages in health and disease are poorly characterized or even completely unknown (4, 5).

Tissue-resident macrophages in adult organisms originate from embryonic progenitors, adult bone marrow (BM), or a mixture of both (6–12). During development, hematopoiesis begins in the yolk sac, giving rise to erythrocytes and macrophages directly and to erythro-myeloid progenitors (EMPs) (6, 13, 14). As hematopoiesis declines in the yolk sac, an intraembryonic wave of definitive hematopoiesis begins in the aorta-gonad-mesonephro, generating hematopoietic stem cells (HSCs). EMPs and then HSCs colonize the fetal liver to give rise to fetal liver monocytes, macrophages, and other immune cells, whereas only HSCs migrate to the BM to establish hematopoiesis in postnatal animals (15). Embryo-derived macrophages can either self-maintain and persist into adulthood or undergo replacement by circulating monocytes at tissue-specific

rates. For example, a majority of macrophages in the gut are continuously replenished by BM-derived cells, whereas brain macrophages, or microglia, are long-lived yolk sac–derived cells that are not replaced in steady-state conditions (8, 14, 16, 17). In certain conditions, origin influences macrophage behavior; for example, following myocardial infarction, embryonic-derived cardiac macrophages promote tissue repair, whereas BM-derived macrophages induce inflammation (18). However, macrophage functions are also imprinted by their microenvironment (19, 20). In the small intestine, macrophages in the muscle express higher levels of tissue-protective genes, such as *Retnla*, *Mrc1*, and *Cd163* compared to lamina propria macrophages, although both originate from adult BM (21).

While the origin and maintenance of bladder-resident macrophages are currently unknown, these macrophages do play a role in response to urinary tract infection (UTI), which affects up to 50% of all women at some point in their lifetimes (5, 22). The immune response to uropathogenic *Escherichia coli* (UPEC) infection in the bladder is characterized by robust cytokine expression leading to rapid infiltration of large numbers of neutrophils and classical Ly6C$^+$ monocytes (23–28). Although essential to bacterial clearance, neutrophil and monocyte infiltration likely also induce collateral tissue damage. Targeted depletion of one of these two cell types is associated with reduced bacterial burden after primary infection in mice, whereas elimination of both cell types together leads to unchecked bacteria growth (23, 25, 26). Tissue-resident macrophages also take up a large number of bacteria during UTI; however, depletion of resident macrophages just before infection does not change bacterial clearance in a first or primary UTI (23). The absence of macrophages in the early stages of a primary UTI significantly improves bacterial clearance during a second, or challenge, infection (23). Exactly how the elimination of resident macrophages improves the response to a challenge infection is unclear, particularly as tissue-associated macrophages return to homeostatic numbers in the time interval between the two infections. Of note, improved bacterial clearance is lost in macrophage-depleted mice that are also

¹Department of Immunology, Institut Pasteur, 75015 Paris, France. ²INSERM U1223 Paris, France. ³Bioinformatic and Biostatistic Hub, Department of Computational Biology, Institut Pasteur, USR 3756 CNRS, Paris, France. ⁴Biomics Platform, Center for Technological Resources and Research (C2RT), Institut Pasteur, Paris, France. ⁵Aix Marseille University, CNRS, INSERM, CIML, Marseille, France. ⁶Macrophages and Endothelial Cells, Department of Developmental and Stem Cell Biology, CNRS UMR3738, Department of Immunology, Institut Pasteur, Paris, France.
*Present address: Centre for Inflammation Research, University of Edinburgh, Edinburgh, UK.
†Corresponding author. Email: molly.ingersoll@pasteur.fr

depleted of CD4$^+$ and CD8$^+$ T cells, suggesting that macrophages modulate T cell activation or limit differentiation of memory T cells, as observed in other tissues (29–33). For example, ablation of embryonic-derived alveolar macrophages results in increased numbers of CD8$^+$ resident memory T cells following influenza infection in mice (31). In the gut, monocyte-derived macrophages support the differentiation of CD8$^+$ tissue-resident memory T cells by production of interferon-β (IFN-β) and interleukin-12 (IL-12) during *Yersinia* infection (32). The opposing roles of macrophages in modulating T cell responses in the lung and gut support the idea that tissue type and/or ontogeny determines how macrophages may influence adaptive immunity (13).

To understand the role of bladder-resident macrophages, we investigated the origin, localization, and function of these cells during infection. We identified two subpopulations of resident macrophages in naïve mouse bladders with distinctive cell surface proteins, spatial distribution, and gene expression profiles. We found that bladder macrophage subsets were long-lived cells, slowly replaced by BM-derived monocytes over the lifetime of the mouse. During UTI, the macrophage subsets differed in their capacity to take up bacteria and survive infection; however, both subsets were replaced by BM-derived cells following resolution of infection. Thus, after a first infection, macrophage subsets had divergent transcriptional profiles compared to their naïve counterparts, shaping the response to subsequent UTI.

RESULTS

Two spatially distinct macrophage populations reside in the naïve bladder

We reported that macrophage depletion before a first UTI improves bacterial clearance during challenge infection (23). Thus, we initiated a follow-up study to investigate the role of bladder-resident macrophages during UTI. Using the macrophage-associated cell surface proteins CD64 and F4/80 (34, 35), we identified a clear CD64 and F4/80 double-positive resident macrophage population in naïve bladders from 7- to 8-week-old female CX$_3$CR1$^{GFP/+}$ mice. This transgenic mouse is widely used to distinguish macrophage populations in other tissues as the chemokine receptor CX$_3$CR1 is expressed by monocytes and macrophages at some point in their development (36). In most tissues, resident macrophages are either GFP$^+$ as they express CX$_3$CR1 or GFP$^-$ because they no longer express CX$_3$CR1 (10). Therefore, we were surprised to observe heterogeneity in green fluorescent protein (GFP) expression levels, revealing potentially two subpopulations (Mac^{lo} and Mac^{hi}) of CD64$^+$ F4/80$^+$ macrophages in the bladder (Fig. 1A). Although the differences were small in magnitude, the Mac^{hi}-expressing population was present in statistically significantly greater numbers and proportions compared to the Mac^{lo} population (Fig. 1A). As CX$_3$CR1 deficiency results in decreased macrophage numbers and frequency in the intestine and brain, and the transgenic CX$_3$CR1$^{GFP/+}$ mouse we used is hemizygous for this receptor (36–38), we investigated whether our putative bladder-resident macrophage subsets were similarly present in wild-type C57BL/6 mice. Using the same gating strategy and an anti-CX$_3$CR1 antibody, we clearly identified that CX$_3$CR1 expression levels distinguished two distinct macrophage populations in 7- to 8-week-old naïve female wild-type mice (Fig. 1B). Notably, wild-type mice had similar numbers and proportions of each macrophage subset (Fig. 1B).

Next, we assessed the surface expression level of proteins known to define macrophage subsets in other tissues (39). We observed that the efferocytic receptor TIM4 and hyaluronan receptor LYVE1 were expressed by the Mac^{lo} population, whereas the Mac^{hi} population was TIM4$^-$ and LYVE1$^-$ (Fig. 1C). Macrophage-associated proteins, such as CD64, F4/80, CD11b, CD11c, and MHC II, were differentially expressed between the subsets (fig. S1A), supporting the notion that these are distinct populations. A recent publication described several organs as having two distinct macrophage subsets, differentiated by their expression of LYVE1, CX$_3$CR1, and, in particular, MHC II (39). To determine whether bladder macrophage subsets represented these two cell types, we used a similar gating strategy (fig. S1B); however, we observed that MHC II$^-$ CD64$^+$F4/80$^+$ cells made up a very minor proportion (<2%) of bladder-resident macrophages (fig. SC). Last, to determine whether additional heterogeneity existed within the CD64$^+$ F4/80$^+$ bladder-resident macrophage population, we used the dimension reduction analyses tSNE and UMAP to visualize our data. In our analyses of the naïve CD45$^+$ cell population, a large CD64$^+$ cluster contained two putative subsets that corresponded to traditionally gated Mac^{lo} and Mac^{hi} populations and included the tiny proportion of MHC II$^-$ macrophages (fig. S1D). tSNE (t-distributed stochastic neighbor embedding) and, more particularly, UMAP (uniform manifold approximation and projection) analysis of CD64$^+$ F4/80$^+$ macrophages revealed two groups, with differential expression of CX$_3$CR1, F4/80, CD64, LYVE1, and TIM4, reflecting the data shown in the traditionally gated histograms (fig. S1, D and E). Thus, we concluded that two subsets of macrophages reside in naïve mouse bladders with differential surface protein expression.

To determine the spatial orientation of the subsets, we stained naïve female C57BL/6 bladders with antibodies to F4/80 and LYVE1 and phalloidin to demarcate the muscle layer from the lamina propria (Fig. 1D). We quantified the number of each subset in these two anatomical locations, observing a higher percentage of the LYVE1$^+$ Mac^{lo} macrophage subset in the muscle compared to the LYVE1$^-$ Mac^{hi} macrophage subset (Fig. 1E). Macrophages in the lamina propria were predominantly of the Mac^{hi} phenotype (Fig. 1E). Thus, the phenotypic differences we observed in bladder-resident macrophage subsets extended to differential tissue localization. Given their spatial organization, we renamed the Mac^{lo} subset "MacM" for muscle and the Mac^{hi} subset "MacL" for lamina propria. Together, these results reveal that two phenotypically distinct macrophage subsets reside in different regions of the naïve bladder.

Bladder-resident macrophages are replaced by HSC-derived macrophages after birth

We next investigated whether macrophage heterogeneity in adult mouse bladders arose due to distinct developmental origins of the subsets. We analyzed bladders from newborn C57BL/6 pups by confocal imaging and by flow cytometry from CX$_3$CR1-GFP–expressing E16.5 (embryonic day 16.5) embryos and newborn mice. We observed that, in E16.5 and newborn animals, a single CX$_3$CR1^{hi} macrophage population was present in the muscle and lamina propria of the bladder. By flow cytometry, these cells were uniformly positive for CD64 and negative for MHC II as expected for fetal macrophages (40) and stained positively for LYVE1 in confocal images of newborn mouse bladder, supporting that diversification of bladder macrophage subsets occurs after birth (Fig. 2A).
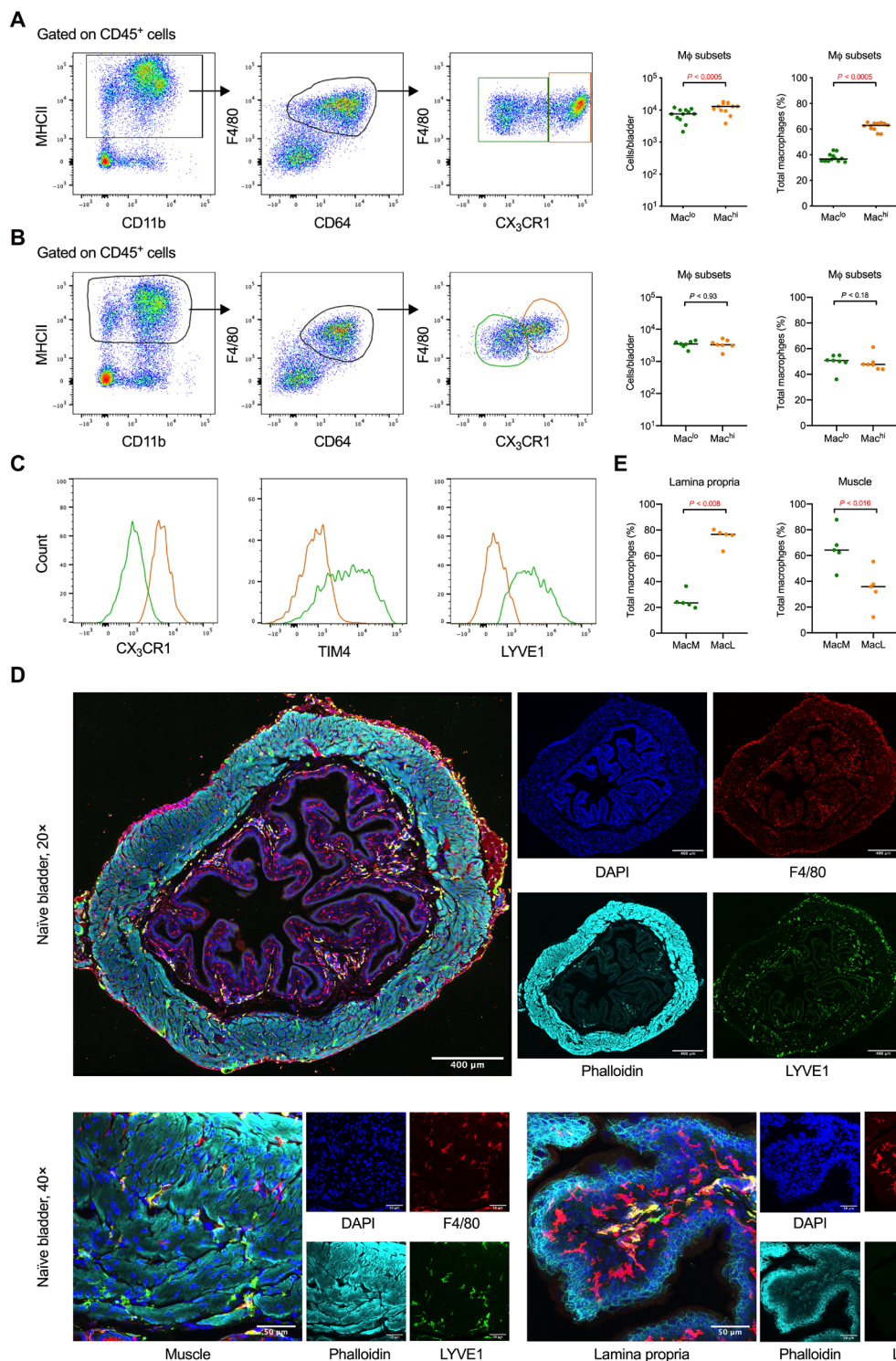
Fig. 1. Two macrophage subsets are resident in adult naïve mouse bladders. (**A** to **C**) Bladders from 7-week-old female CX$_3$CR1$^{GFP/+}$ and C57BL6/J mice were analyzed by flow cytometry. (A and B) Dot plots depict the gating strategy for macrophages subsets and graphs show the total cell number (log scale, left) and proportion (right) of bladder macrophage subset, derived from cytometric analysis in (A) CX$_3$CR1$^{GFP/+}$ and (B) C57BL6/J mice. (C) Histograms show the relative expression of CX$_3$CR1, TIM4, and LYVE1 on macrophage subsets in C57BL6/J, Mac^{lo} is green and Mac^{hi} is orange. (See fig. S1 for data on expression of additional proteins). (**D**) Representative confocal images of bladders from C57BL6/J mice at 20× and 40×. Merged images and single channels with the target of interest are shown. DAPI, 4′,6-diamidino-2-phenylindole. (**E**) Graphs show the proportion of each macrophage subset in the lamina propria and muscle of naïve C57BL6/J mice. Data are pooled from three experiments, $n = 3$ to 6 mice per experiment. Each dot represents one mouse; lines are medians. Significance was determined using the nonparametric Mann-Whitney test to compare macrophage subset numbers (A and B) and the nonparametric Wilcoxon matched-pairs signed-rank test to compare the macrophage subset percentages (A, B, and E). All P values are shown; statistically significant P values (<0.05) are in red.
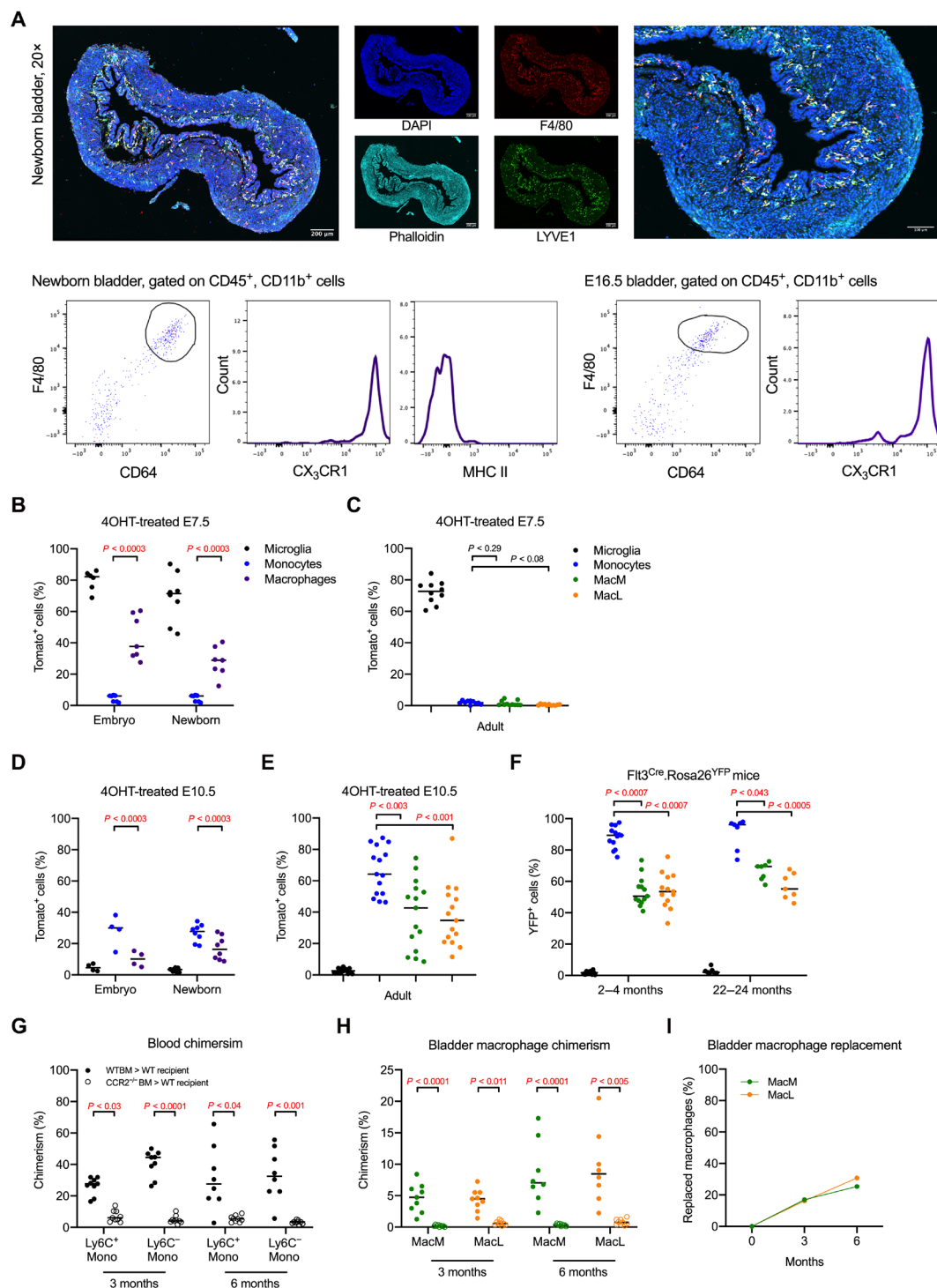
Fig. 2. Bladder-resident macrophages are long-lived HSC-derived cells. (**A**) Merged confocal and single channel images from a C57BL/6 newborn mouse bladder. Left image is enlarged at the right. Gating strategy in *Cdh5*-CreERT2Rosa26[tdTomato] CX₃CR1[GFP] newborn mice and E16.5 embryos; histograms show CX₃CR1 and MHC II expression. (**B** to **E**) Reporter recombination in microglia, monocytes, bladder macrophages, and MacM and MacL subsets in *Cdh5*-CreERT2Rosa26[tdTomato] mice: (B) E16.5 embryos, newborns 4-hydroxytamoxifen (4OHT)-treated at E7.5, (C) adults 4OHT-treated at E7.5, (D) E16.5 embryos, newborns 4OHT-treated at E10.5, (E) adults 4OHT-treated at E10.5. (**F**) Percentage of YFP⁺ cells in microglia, monocytes, MacM, and MacL macrophages in adult Flt3[Cre]Rosa26[YFP] mice. (**G** to **I**) Adult shield-irradiated C57BL/6 CD45.2 mice reconstituted with CCR2^{+/+} CD45.1 BM and C57BL/6 CD45.1 mice reconstituted with CCR2^{−/−} CD45.2 BM. Percentage of donor cells (G) in monocytes or (H) bladder-resident macrophages in mice transplanted with CCR2^{+/+} or CCR2^{−/−} BM at 3 and 6 months after transplantation. (See fig. S2 for data on blood leukocyte chimerism). (I) Bladder-resident macrophage replacement rate. Data pooled from two to three experiments, *n* = 2 to 6 mice per experiment. Each point represents one mouse; lines are medians. Significance determined using the Mann-Whitney test comparing (B to F) macrophages or subsets to monocytes or (G and H) CCR2^{+/+} to CCR2^{−/−} recipients, *P* values were corrected for multiple testing using the false discovery rate (FDR) method. All *P* values are shown; statistically significant *P* values (<0.05) are in red.

We hypothesized that, in adult mice, macrophage subsets arise following differentiation of cells seeded from embryonic progenitors or that one subset is derived from embryonic macrophages, whereas the second subset arises from BM-derived monocytes (*41*). To test these hypotheses, we used the *Cdh5*-CreERT2 Rosa26[tdTomato] transgenic mouse, in which the contribution of distinct hematopoietic progenitor waves to immune cell populations can be followed temporally, such that treatment of pregnant mice with 4-hydroxytamoxifen (4OHT) at E7.5 labels yolk sac progenitors and their progeny and treatment at E10.5 labels HSC that will settle in the BM (adult-type HSCs) and their cellular output (*42*). After treatment with 4OHT at E7.5, in which microglia were labeled as expected (*8*, *14*), we found a significantly higher proportion of labeled bladder macrophages compared to monocytes in E16.5 embryos and newborn mice (Fig. 2B). Labeled bladder macrophage subsets were nearly absent, similar to monocytes, in adult (8- to 11-week-old) mice (Fig. 2C). These data support the fact that yolk sac–derived bladder macrophages are diluted after birth in the adult and suggest that the subsets are composed of HSC-derived macrophages. Low levels of E10.5-labeled macrophages were detected in embryonic bladders (Fig. 2D), and their frequency increased in newborn and adult mice, although to a lesser degree than monocytes, supporting the idea that bladder macrophage subsets arise, at least in part, from adult-type HSCs (Fig. 2, D and E). Of note, both subsets found in the adult bladder showed similar frequencies of E10.5 labeling (Fig. 2E). Together, these results demonstrate that adult bladder macrophages are partially HSC-derived and the macrophage subsets cannot be distinguished from each other by their ontogeny.

To confirm that HSC-derived progenitors contribute to the bladder-resident macrophage pool, we analyzed bladders from adult Flt3[Cre] Rosa26[YFP] mice. In this transgenic mouse, expression of the tyrosine kinase receptor Flt3 in multipotent progenitors leads to expression of yellow fluorescent protein (YFP) in the progeny of these cells, such as monocytes, whereas microglia, arising from yolk sac progenitors, are essentially YFP[−] (*43*). Recombination rates driven by Flt3 are very low during embryonic development, but blood monocyte labeling reaches 80 to 90% in adult mice (*7*). Therefore, if tissue-resident macrophages arise from postnatal BM-derived monocytes, labeling in adult mice should be similar to blood monocytes, whereas the presence of Flt3^{−} tissue macrophages would indicate that they originated from either embryonic HSCs or adult Flt3-independent progenitors. We observed that, in 2- to 4-month-old and 22- to 24-month-old mice, ~50% of each macrophage subset was YFP[+], which was significantly lower compared to circulating monocytes (Fig. 2F). This observation and those from the *Cdh5*-CreERT2 mice together support the fact that, in addition to adult HSCs, adult bladder macrophage subsets are derived from embryonic progenitors that may include fetal HSCs, and/or later yolk sac progenitors, but with no contribution from early yolk sac progenitors. In addition, the lack of equilibration of YFP labeling in the bladder with blood monocytes at 22 to 24 months suggests that tissue macrophages are not rapidly replaced over the lifetime of the mouse by BM-derived cells in the context of homeostasis.

To determine the replacement rate of bladder-resident macrophages by BM-derived cells in the adult mouse, we evaluated shielded irradiated mice, in which adult animals are irradiated with a lead cover over the bladder to protect this organ from radiation-induced immune cell death and nonhomeostatic immune cell infiltration.

Animals were transplanted with congenic BM from wild-type or CCR2^{−/−} mice. Monocytes depend on CCR2 receptor signaling to exit the BM into circulation (*44*). At 3 and 6 months, we observed that a median of 27.7% (3 months) and 27.6% (6 months) of circulating Ly6C^{+} monocytes were of donor origin in mice reconstituted with wild-type BM, which is well in-line with published studies using this approach (*45*, *46*), whereas only 6.1% (3 months) and 6.5% (6 months) of Ly6C^{+} monocytes were of donor origin in wild-type mice receiving CCR2^{−/−} BM (Fig. 2G). B and natural killer (NK) cells were replenished to a greater extent in mice reconstituted with CCR2^{−/−} BM compared to mice reconstituted with CCR2^{+/+} BM, which could be due to different engraftment efficiencies between CD45.1 and CD45.2 BM (fig. S2) (*47*, *48*). In mice reconstituted with wild-type BM, 4.7% of MacM and 4.5% MacL were of donor origin at 3 months after engraftment. At 6 months after irradiation, 7% of MacM and 8.5% of MacL macrophages were of donor origin (Fig. 2H). Chimerism in bladder macrophage subsets was markedly reduced in CCR2^{−/−} BM recipients, suggesting that monocytes slowly replace bladder macrophage subsets in a CCR2-dependent manner (Fig. 2H). By dividing the median macrophage subset chimerism (7 or 8.5%) by the median circulating Ly6C^{+} monocyte chimerism at 6 months in mice receiving wild-type BM (27.6%), we determined that 25.3% of MacM and 30.8% MacL were replaced by BM-derived monocytes within 6 months (Fig. 2I).

Together, these results reveal that the establishment of distinct bladder-resident macrophage subsets occurs postnatally. Yolk sac macrophages initially seed the fetal bladder but are replaced by fetal HSC-derived macrophages. In adult mice, bladder macrophage subsets are partially maintained through a slow replacement by BM-derived monocytes, although a substantial number of fetally derived cells remain. The incomplete macrophage labeling we observed in our experiments supports the idea that a progenitor source, which cannot be labeled in either model, contributes to resident bladder macrophages. Currently, there is no fate-mapping model to discriminate or follow progeny specifically from late yolk sac EMPs or early fetally restricted HSC, as hematopoietic waves overlap in development. We can conclude that MacM and MacL macrophages do not differ in their developmental origin or rate of replacement by monocytes, supporting the view that one or more unique niches in adult tissue may be responsible for macrophage specialization into phenotypical and functionally distinct macrophage subsets.

Bladder-resident macrophage subsets have divergent transcriptomes

Although bladder-resident macrophage subsets had similar ontogeny, their distinct spatial localization and surface protein expression suggested that they have different functions. To test this hypothesis, we first analyzed gene expression profiles of naïve adult female MacM and MacL macrophages using bulk RNA sequencing (RNA-seq) (fig. S3A, gating strategy). To formally demonstrate that our cells of interest are macrophages, we aligned the transcriptomes of the bladder macrophage subsets with the macrophage core signature list published by the Immunological Genome Consortium and the bladder macrophage core list from the mouse cell atlas single-cell database (*35*, *49*). The MacM and MacL subsets expressed 80% of the genes from the Immunological Genome Consortium macrophage core signature list and more than 95% of the genes in the bladder macrophage core list (fig. S3B), supporting the idea

that our cells of interest are fully differentiated tissue-resident macrophages.

We observed that 1475 genes were differentially expressed between naïve MacM and MacL macrophages, in which 899 genes were positively regulated and 576 genes were negatively regulated in the MacL subset relative to MacM macrophages (Fig. 3A). In the top 20 differentially expressed genes (DEG), MacM macrophages expressed higher levels of *Tfrc*, *Ms4a8a*, *Serpinb6a*, *CCL24*, *Scl40a1*, *Clec10a*, and *Retnla*, all of which are associated with an alternatively activated macrophage phenotype (*50–53*); genes involved in iron metabolism, such as *Tfrc*, *Steap4*, and *Slc40a1* (*54*); and genes from the complement cascade, including *C4b* and *Cfp* (Fig. 3B). In the same 20 most DEG, MacL macrophages expressed greater levels of *Cx3cr1*, *Cd72*, *Itgb5*, *Axl*, and *Itgav*, which are associated with phagocytosis, antigen presentation, and immune response activation (Fig. 3B) (*55–57*). MacL macrophages also expressed inflammatory genes, such as *Cxcl16*, a chemoattractant for T and NKT cells (*58*, *59*), and *Lpcat2* and *Pdgfb*, which are involved in the metabolism of inflammatory lipid mediators (Fig. 3B) (*60*, *61*). Using gene set enrichment analysis of the DEG to detect pathways up-regulated in the macrophage subsets, we observed that the MacM subset expressed genes linked to pathways such as endocytosis, mineral absorption, lysosome, and phagosome (Fig. 3C). Within the phagosome and endocytosis pathways, genes critical for bacterial sensing and alternative activation such as *Tlr4*, *Mrc1* (encoding for CD206), *Cd209*, and *Egfr* (*62–64*) were increased in the MacM subset. In the mineral absorption pathway, genes controlling iron metabolism that also enhance bacterial killing such as *Hmox1* and *Hmox2* were up-regulated in MacM macrophages (Fig. 3D) (*65*). In the MacL subset, genes linked to diverse inflammatory pathways, including *Toll-like receptor signaling, apoptosis, antigen processing and presentation,* and *chemokine signaling,* were present, as were many infectious and inflammatory disease–related pathways (Fig. 3E). Within these pathways, the MacL subset expressed genes related to bacterial sensing, such as *Tlr1*, *Tlr2*, and *Cd14*; initiation of inflammation, such as *Il1b*, *Tnf*, *Ccl3*, *Ccl4*, *Cxcl10*, *Cxcl16*, and *Nfkb1*; and apoptotic cell death, such as *Mapk8*, *Pmaip1*, *Bcla1d*, *Cflar*, *Bcl2l11*, and *Birc2* (Fig. 3F).

These findings suggest that MacM macrophages are more anti-inflammatory with increased endocytic activity, which is a common feature of highly phagocytic resident macrophages (*66*), and as such may play a prominent role in bacterial uptake or killing during infection. MacL, on the other hand, may play a greater role in antigen presentation and initiation or maintenance of inflammation.

Macrophage subsets respond differently to infection
As we observed enrichment of genes belonging to *endocytosis, lysosome,* and *phagosome* pathways in the MacM subset, we reasoned that the macrophage subsets differentially take up bacteria during infection. To test our hypothesis, we used a well-described mouse model of UTI, in which we transurethrally infect adult female mice via catheterization with 10^7 colony-forming units (CFU) of UPEC strain UTI89-RFP, which expresses a red fluorescent protein (RFP) (*23*). At 24 hours post-infection (PI), we investigated bacterial uptake by macrophage subsets (Fig. 4, A and B). Despite that MacM macrophages are farther from the infected urothelium than MacL macrophages, we observed that 20% of MacM and only 10% of MacL subsets contained bacteria at 24 hours PI, providing functional evidence to support the transcriptional data that MacM

macrophages have a superior phagocytic capacity compared to MacL macrophages (Fig. 4B). Supporting this conclusion, we found that when we exposed sorted MacM and MacL macrophages to live UPEC in vitro, a greater proportion of MacM macrophages internalized bacteria after 2 hours compared to MacL macrophages (fig. S4A). In addition, despite very low levels of infection overall (~1% of macrophages), more UPEC could be found in MacM macrophages compared to MacL macrophages at 4 hours PI in vivo (fig. S4B). Taking the total population of UPEC-containing macrophages at 24 hours PI, we observed that ~80% of these cells were MacM macrophages, whereas the MacL subset comprised only 20% of this population, which was unusual given that MacM and MacL exist in the bladder in a 1:1 ratio (Fig. 4B and fig. S4C, gating strategy).

Given the predominance of genes associated with alternatively activated macrophages in the top 20 DEGs of MacM macrophages (Fig. 3B), we measured polarization of the macrophage subsets in naïve and infected bladders by analyzing the expression of IL-4Rα by flow cytometry (Fig. 4C). IL-4Rα is the receptor of IL-4 and IL-13, two cytokines that drive alternative activation in macrophages (*67*). Both subsets had increased expression of IL-4Rα at 24 hours PI compared to their naïve counterparts; however, MacM macrophages had consistently higher expression levels of IL-4Rα compared to MacL macrophages in naïve and infected tissue (Fig. 4C).

In the course of our studies, we observed that the total number and proportion of MacL macrophages were significantly lower than those of MacM macrophages at 24 hours PI, whereas, in naïve mice, both the number and proportion of the macrophage subsets were equivalent (Figs. 4D and 1B). To rule out the contribution of differentiated monocyte-derived cells to the macrophage pool, we assessed total macrophage cell numbers in the bladder at 4 hours PI, when there is minimal monocyte infiltration (Fig. 4E) (*23*). Macrophage subset numbers and proportions were significantly different at 4 hours PI (Fig. 4F). As the total numbers of each subset were not increased over naïve levels (Fig. 1B), we hypothesized that macrophages die during infection, particularly as apoptosis pathways were more highly expressed in MacL macrophages (Fig. 3, C and D). Using a cell viability dye, which labels dying/dead cells, we found that a significantly higher proportion of MacL macrophages were dying compared to MacM macrophages at 4 hours PI (Fig. 4G and fig. S4D, gating strategy). As UPEC strains can induce macrophage death in vitro (*68*, *69*), we asked whether macrophage cell death was induced by UPEC in vivo. We observed that only 20% of dying or dead cells in each subset were infected (Fig. 4H), suggesting that macrophage death was not primarily driven by UPEC uptake. To determine whether macrophage cell death was confined to a distinct location, we quantified macrophage subset numbers in the muscle and lamina propria. We observed that, at 4 hours PI, only MacL macrophages located in the lamina propria were reduced in numbers compared to naïve mice (Fig. 4I). Given that, in the first hours after infection, the urothelium exfoliates massively (*70*), these results suggest that macrophage death, specifically in the lamina propria, may be due to the loss of a survival factor in this niche. To test whether alteration of the niche induced macrophage death, we chemically induced global urothelial exfoliation by intravesical instillation of protamine sulfate (*71*, *72*). We observed that at 5 hours after treatment, the total numbers of both MacM and MacL subsets were reduced compared to macrophage subsets in naïve mice (fig. S4E), suggesting that alterations in bladder urothelium are
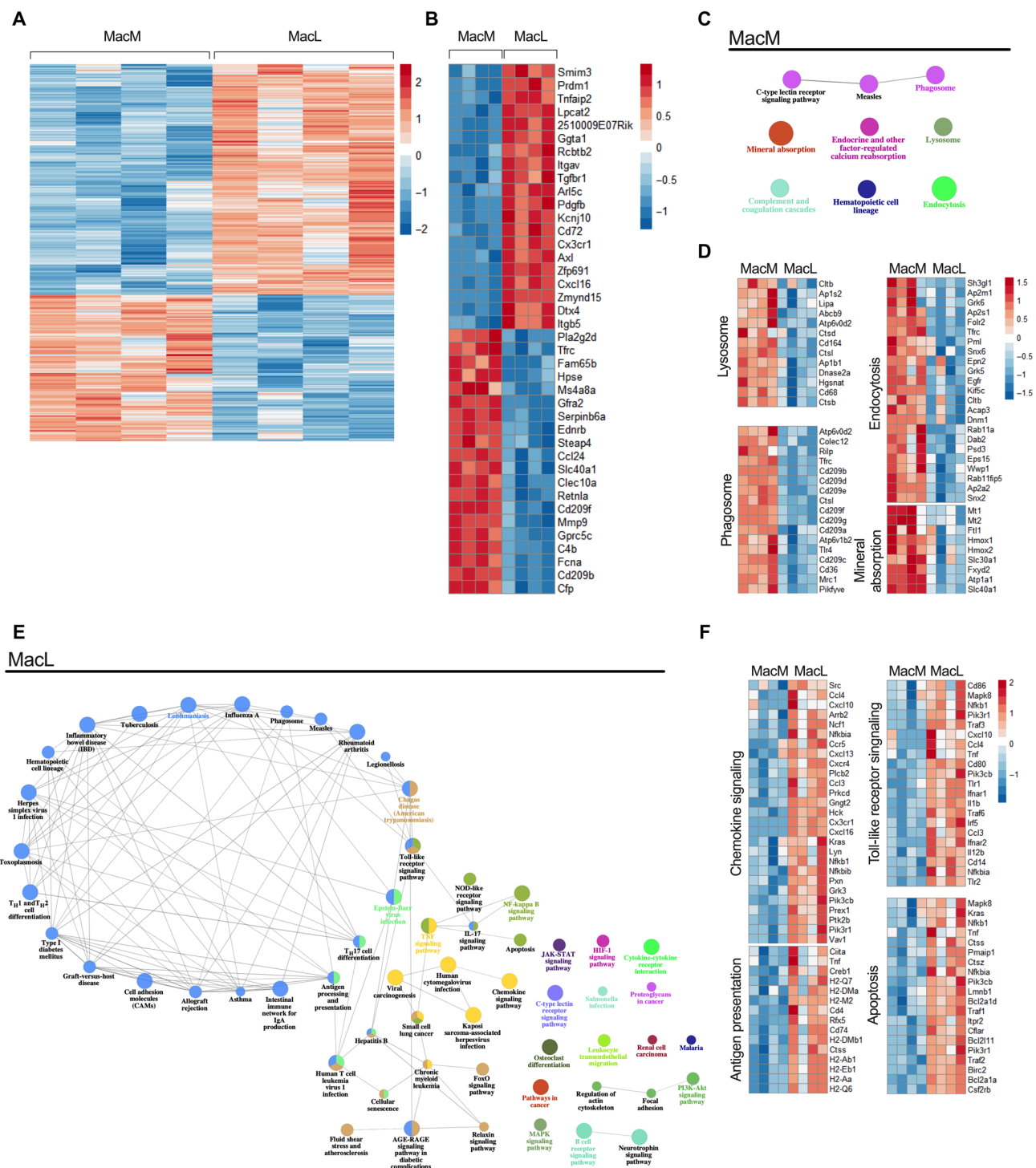
Fig. 3. Naïve macrophage subsets have different transcriptional programs in the naïve bladder. MacM and MacL macrophages were sorted from 7- to 8-week-old female naïve adult C57BL/6 mouse bladders and analyzed by RNA-seq (fig. S3, gating strategy). (**A**) Heatmaps show the gene expression profile of the 1475 differentially expressed genes and (**B**) the 20 most differentially expressed genes between the MacM and MacL subsets. (**C** to **F**) Using Kyoto Encyclopedia of Genes and Genomes (KEGG) pathway analysis of significantly up-regulated genes, the following are depicted: (C) pathways enriched in MacM macrophages, (D) up-regulated genes associated with selected pathways in MacM macrophages, (E) pathways enriched in MacL macrophages, and (F) up-regulated genes associated with selected pathways in MacL macrophages. In (C) and (E), the size of the nodes reflects the statistical significance of the term. ($Q < 0.05$; terms > 3 genes; % genes/term > 3; κ 0.4).
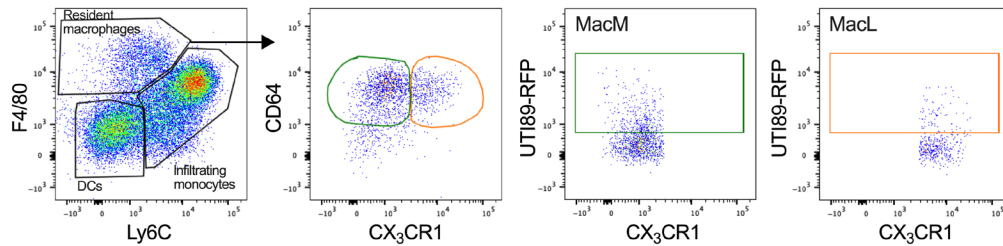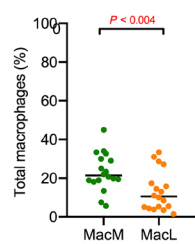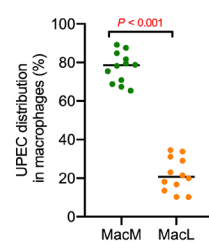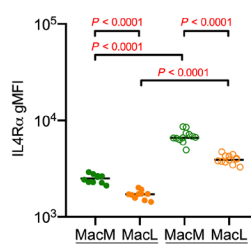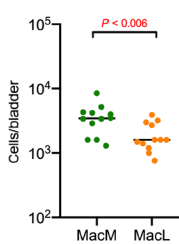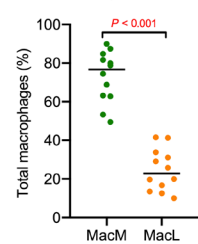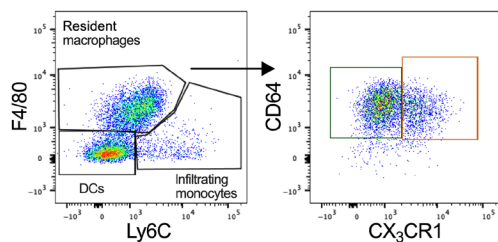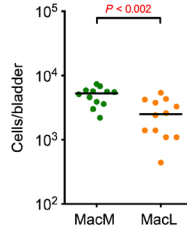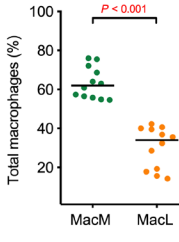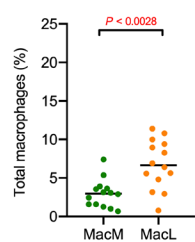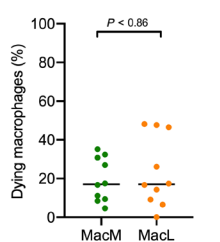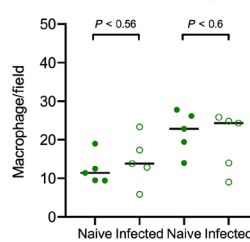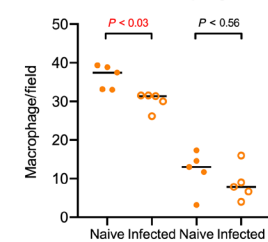
Fig. 4. Macrophage subsets have divergent roles in UTI. (**A** to **H**) Female C57BL6/J mice were infected with UTI89-RFP and bladders were analyzed by flow cytometry at (A to D) 24 hours or (E to H) 4 hours PI. (A) Gating strategy, resident macrophage subsets, and cells containing bacteria. (B) Percentage of infected macrophage subsets and UPEC distribution (fig. S4B, gating strategy). (C) IL-4Rα gMFI (geometric mean fluorescence intensity) in naïve mice and 24 hours PI. (D) Total number and frequency of bladder macrophage subsets. (E) Gating strategy. (F) Total number and frequency of bladder macrophage subsets. Percentage of (G) macrophage subsets labeled with a live/dead marker (fig. S4D, gating strategy) and (H) dying macrophages containing UPEC. (**I**) MacM and MacL macrophage quantification in naïve mice and 4 hours PI. (B to D and F to H) Data pooled from three experiments, *n* = 3 to 6 mice per experiment. (I) Data are pooled from two experiments, *n* = 2 to 3 mice per experiment. Each dot represents one mouse; lines are medians. In (D) and (F), Mann-Whitney test was used to compare the numbers and the nonparametric Wilcoxon matched-pairs signed-rank test was used to compare the percentages of each macrophage subset. (B and C and G to I) Mann-Whitney test. *P* values were corrected for multiple testing using the FDR method. All *P* values are shown; statistically significant *P* values (<0.05) are in red.

sufficient to reduce resident macrophage numbers in the bladder, although protamine sulfate may also directly induce macrophage death. Thus, we functionally validated the divergent gene expression observed between macrophage subsets, in which MacM macrophages are more phagocytic and MacL macrophages are more prone to die, supporting the idea that gene expression differences translate to divergent roles for the subsets in response to UTI.

Monocyte-derived macrophages replace resident macrophage subsets after infection

As we observed macrophages dying during infection, we investigated the change in macrophage numbers over time as animals resolved their infection. Both populations significantly decreased at 24 hours PI, then subsequently increased nearly 10-fold at 7 days PI, and returned to numbers just above homeostatic levels at 4 weeks PI (Fig. 5A). With the dynamic increase of macrophage numbers over the course of UTI, we hypothesized that infiltrating monocytes replace resident macrophage subsets during infection, as we previously reported that infiltrating monocytes differentiate to cells resembling macrophages at 48 hours PI (23). To test this hypothesis, we used the CCR2^{CreERT2} Rosa26^{tdTomato} mouse, in which administration of 4OHT induces recombination in CCR2-expressing cells, such as circulating Ly6C$^+$ monocytes, leading to irreversible labeling of these cells in vivo (73). Blood monocytes and bladder-resident macrophages are not Tomato$^+$ in untreated mice (fig. S5). We administered 4OHT to naïve mice and, then, 24 hours later, infected half of the treated mice with 10^7 CFU of UTI89. At this time point, 24 hours after 4OHT treatment, we analyzed the labeling efficiency in circulating classical Ly6C$^+$ monocytes, finding that approximately 80% of Ly6C$^+$ monocytes were labeled in both naïve and infected mice (Fig. 5B). After 6 weeks, when animals had resolved their infection, there were no labeled circulating Ly6C$^+$ monocytes in naïve or post-infected mice (Fig. 5B). When we analyzed the bladders of naïve mice 6 weeks after the 4OHT pulse, only 2.9% of MacM and 2.1% of MacL macrophage subsets were labeled, supporting our earlier conclusion that monocytes contribute to bladder macrophage subsets at a very slow rate in the steady state (Fig. 5C). At 6 weeks PI, the total numbers of macrophage subsets finally returned to homeostatic levels (Fig. 5D), but PI MacM and MacL macrophages had two to three times more Tomato$^+$ cells (median, MacM 8.4%, MacL 4.4%) than their naïve counterparts. These data support the fact that, after monocytes infiltrate the bladder during infection, they remain in the tissue following resolution, integrating themselves into the resident macrophage pool, and thus contribute to the return of macrophage subsets to homeostatic levels.

As monocytes generally have different origins and developmental programs compared to tissue-resident macrophages, we used RNA-seq to determine whether the macrophage pool in post-infected bladders was different from naïve tissue-resident cells. Using principal component analysis (PCA), we compared bladder macrophage subsets from 6-week post-infected mice to their naïve counterparts. We found that macrophages clustered more closely together by subset, rather than by infection status, or, in other words, naïve and post-infected MacL macrophages clustered more closely to each other than either sample clustered to naïve or post-infected MacM macrophages (Fig. 5E). Five hundred thirteen genes (247 genes down-regulated and 266 genes up-regulated) were different between naïve and post-infected MacM macrophages (Fig. 5F). Six hundred seventeen genes (401 genes down-regulated

and 216 genes up-regulated) were differentially expressed between the naïve and post-infected MacL subset (Fig. 5G). Applying gene set enrichment analysis to up-regulated genes in the post-infected macrophage subsets, we detected common pathways between the subsets including enrichment of genes linked to pathways such as *antigen presentation*; *cell adhesion molecules*; *T$_H$1, T$_H$2, and T$_H$17 cell differentiation*; and *chemokine signaling pathway* (Fig. 5, H and I). Although the enriched genes were not identical within each subset for these pathways, some common up-regulated genes included those encoding for histocompatibility class 2 molecules, such as *H2-Ab1*, *H2-Eb1*, *H2-DMb1*, *Ciita*, and the Stat1 transcription factor (Fig. 5, I and J). As differentiation of monocytes into macrophages includes up-regulation of cell adhesion and antigen presentation molecules (74), including in the bladder (23), these data further support the idea that monocytes specifically contribute to the PI bladder-resident macrophage pool.

These results show that, in the context of UTI, dying macrophages are replaced by monocyte-derived cells. Tissue-resident macrophage subsets maintain their separate identities distinct from each other after infection, although each subset also takes on a different transcriptional profile compared to their naïve counterparts, with up-regulated expression of genes related to adaptive immune responses.

Macrophage depletion before challenge improves bacterial clearance

We previously reported that macrophage depletion 24 hours before a primary UTI does not affect bacterial clearance (23). Given that post-infected macrophage subsets up-regulated pathways different from those associated with the transcriptomes of naïve bladder macrophage subsets, and that these pathways were linked to inflammatory diseases and the adaptive immune response, we hypothesized that one or both macrophage subsets would mediate improved bacterial clearance to a challenge infection. To test this hypothesis, we infected mice with 10^7 CFU of kanamycin-resistant UTI89-RFP. Four weeks later, when the infection was resolved, mice were challenged with 10^7 CFU of the isogenic ampicillin-resistant UPEC strain, UTI89-GFP, and bacterial burden was measured at 24 hours PI. To test the contribution of the macrophage subsets to the response to challenge infection, we used different concentrations of anti-CSF1R depleting antibody to differently target the two macrophage subsets directly before challenge infection (Fig. 6A, experimental scheme). Using 500 μg of anti-CSF1R antibody, we depleted 50% of MacM and 80% of MacL macrophages, whereas depletion following treatment with 800 μg of anti-CSF1R antibody reduced MacM macrophages by 80% and the MacL subset by more than 90% (Fig. 6B and fig. S6A). Twenty-four hours after anti-CSF1R antibody treatment, the number of circulating neutrophils, eosinophils, NK, B, or T cells was not different from mock-treated mice at either concentration (fig. S6B). Classical Ly6C$^+$ monocytes were modestly reduced in mice treated with 800 μg of anti-CSF1R antibody but were unchanged in mice receiving 500 μg of depleting antibody. Antibody treatment did not change circulating nonclassical monocyte numbers (fig. S6B). After challenge infection, the bacterial burden was not different in mice treated with 500 μg of anti-CSF1R compared to mock-treated mice (Fig. 6C). By contrast, mice depleted with 800 μg of anti-CSF1R had reduced bacterial burdens, indicative of a stronger response after challenge compared to nondepleted mice (Fig. 6D).
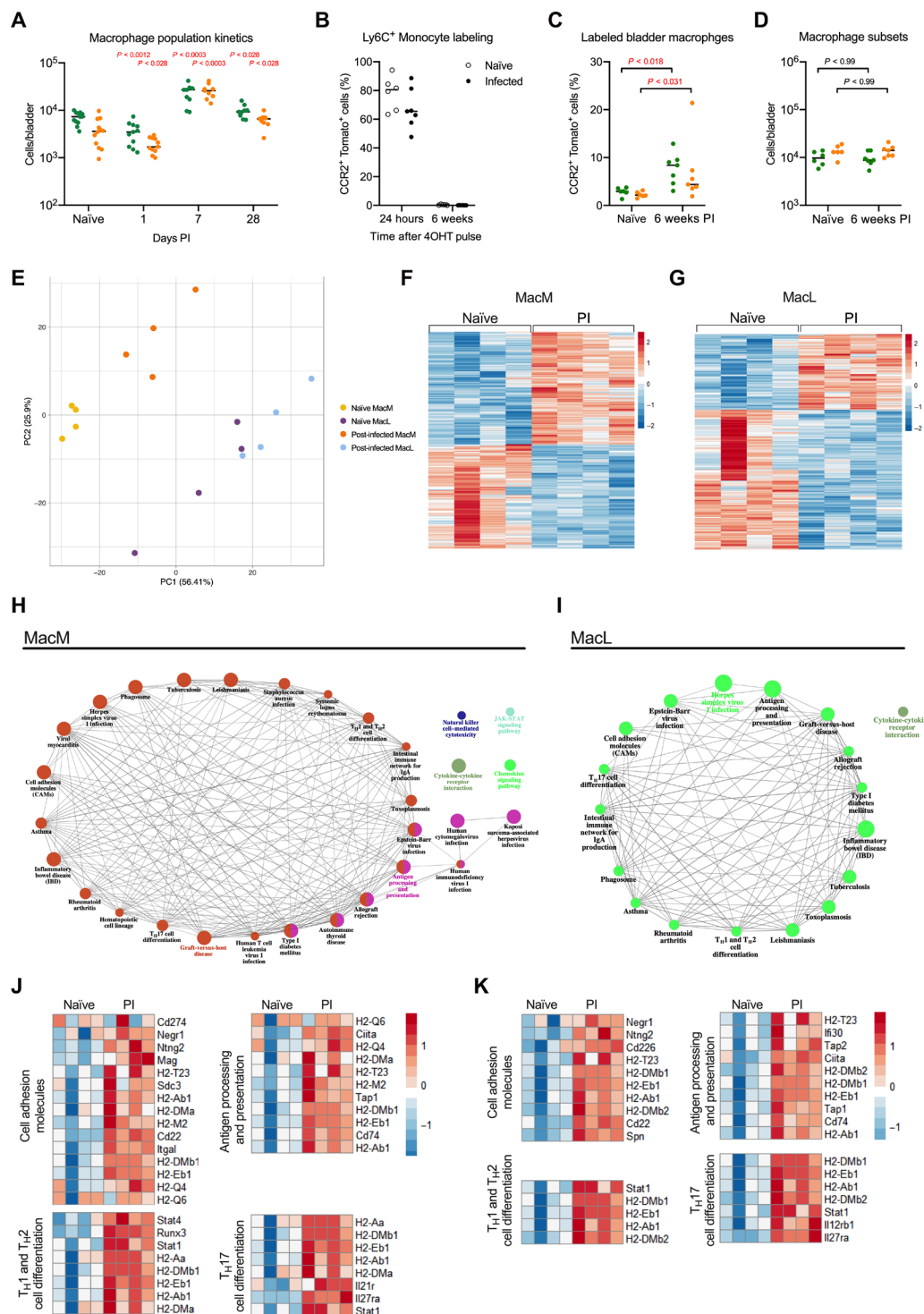
Fig. 5. Macrophage subset transcriptional profiles are altered by UTI. (**A**) Total number of MacM (green) and MacL (orange) in naïve and 1-, 7-, or 28-day PI mice. (**B** and **C**) CCR2^{CreERT2}Rosa26^{tdTomato} mice were pulsed with 4OHT. Twenty-four hours later, half were infected with UTI89-RFP. Percentage of Tomato$^+$ (B) Ly6C$^+$ monocytes 24 hours and 6 weeks after 4OHT-pulse or (C) bladder macrophage subsets 6 weeks after 4OHT-pulse. (**D**) Total number of macrophage subsets in naïve and 6-week PI bladders. (**E**) Replicate-adjusted principal component analysis of all genes from naïve and post-infected bladder macrophage subsets. Differentially expressed genes between naïve and 6-week PI (**F**) MacM (513 genes) and (**G**) MacL (617 genes) macrophages. KEGG pathway analysis of significantly up-regulated genes, enriched in 6-week PI (**H**) MacM and (**I**) MacL macrophages. Up-regulated genes from selected pathways in 6-week PI (**J**) MacM and (**K**) MacL macrophages. (A, C, and D) Mann-Whitney test comparing infection to naïve. P values were corrected for multiple testing using the FDR method. Higher left-shifted P values refer to MacM and lower right-shifted P values refer to MacL. (H and I) Node size reflects statistical significance of the term ($Q < 0.05$; terms > 3 genes; %genes/term > 3; κ 0.4). All P values are shown; statistically significant P values (<0.05) are in red.
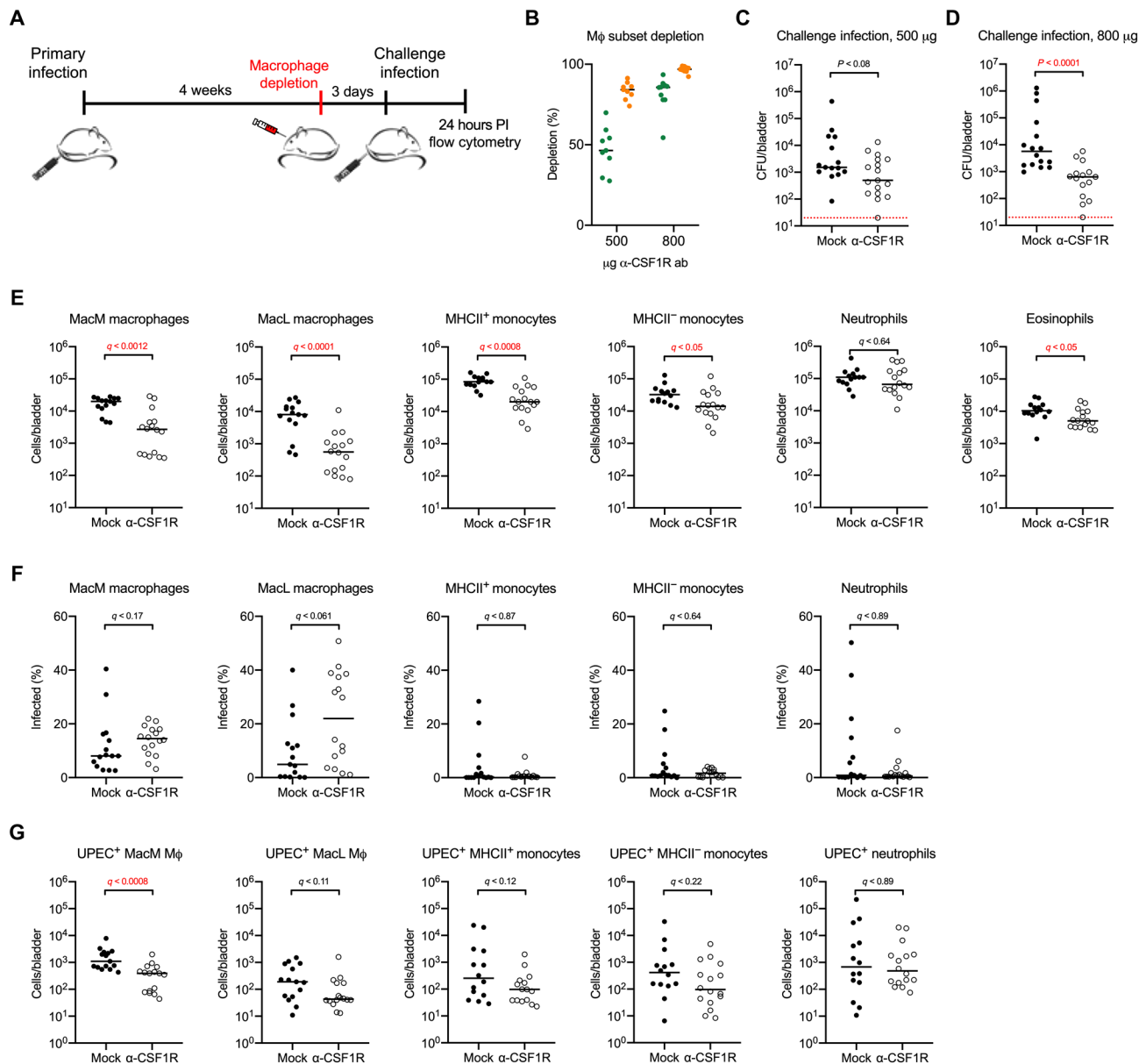
Fig. 6. Macrophage depletion before challenge infection promotes improved bacterial clearance. (**A**) Experimental scheme. (**B**) Efficacy of macrophage subset depletion in naïve C57BL/6 mice treated with 500 or 800 μg of anti-CSF1R antibody. (**C** and **D**) Bacterial burden per bladder 24 hours after challenge in female C57BL/6 mice infected with UTI89-RFP according to (A) and treated with phosphate-buffered saline (PBS) (mock) or (C) 500 μg or (D) 800 μg of anti-CSF1R antibody 72 hours before being challenged with the isogenic UTI89-GFP strain. (**E** to **G**) Mice were infected according to (A) and treated with 800 μg of anti-CSF1R antibody 72 hours before challenge infection with 10^7 CFU of the isogenic UTI89-GFP strain. Graphs depict the (E) total number of the indicated cell type, (F) the percentage of the indicated cell type that was infected, and (G) the total number of the indicated cell type that contained UPEC at 24 hours after challenge in mice treated with PBS or 800 μg of anti-CSF1R antibody. Data are pooled from three experiments, $n = 3$ to 6 mice per experiment. Each dot represents one mouse; lines are medians. (C to G) Mann-Whitney test, P values were corrected for multiple testing using the FDR method. All P values are shown; statistically significant P values (<0.05) are in red.

Neutrophils take up a majority of UPEC at early time points during UTI (*23*). Therefore, we hypothesized that the improved bacterial clearance in macrophage-depleted mice may be due to increased infiltration of inflammatory cells, such as neutrophils. At 24 hours after challenge infection, we observed that, while the numbers of resident macrophage subsets, MHCII⁺ monocytes, and MHCII⁻ monocytes in macrophage-depleted mice were reduced compared to mock-treated mice, as expected, the numbers of infil-

trating neutrophils were unchanged by antibody treatment (Fig. 6E and fig. S6C, gating strategy). Fewer eosinophils infiltrated the tissue in macrophage-depleted mice, although the impact of this is unclear as their role in infection is unknown (Fig. 6E). Given that neutrophil infiltration was unchanged and that monocytes, which also take up a large number of bacteria during infection, were reduced in number, we considered that improved bacterial clearance in macrophage-depleted mice may be due to increased bacterial

uptake on a per-cell basis during challenge infection. However, bacterial uptake was not different between depleted and mock-treated mice in neutrophils, MHCII$^+$ and MHCII$^-$ monocytes, or either macrophage subset (Fig. 6F). The lower numbers of the MacM subset in macrophage-depleted mice translated to lower numbers of infected MacM macrophages (Fig. 6, E and G, respectively). However, we observed no differences in the numbers of infected MacL macrophages, neutrophils, and MHCII$^+$ or MHCII$^-$ monocytes in macrophage-depleted mice compared to nondepleted animals (Fig. 6G). Together, these results support the notion that MacM macrophages negatively affect bacterial clearance in a challenge infection, but not at the level of direct bacterial uptake or myeloid cell infiltration.

Depleting macrophages leads to a T$_H$1-biased immune response during challenge infection

As infiltration of inflammatory cells or the number of infected cells during challenge infection was not changed in macrophage-depleted mice, we questioned whether another host mechanism was involved in bacterial clearance. Exfoliation of infected urothelial cells is a host mechanism to eliminate bacteria (70, 75). We hypothesized that macrophage-depleted mice have increased urothelial exfoliation during challenge infection, leading to reduced bacterial numbers. We quantified the mean fluorescence intensity of uroplakins, proteins expressed by terminally differentiated urothelial cells (76), from bladders of post-challenged mice, depleted of macrophages or not (Fig. 7A). We did not detect a significant difference in urothelial exfoliation between mock-treated animals and mice depleted of macrophage before challenge infection, supporting that urothelial exfoliation is not the underlying mechanism behind improved bacterial clearance in macrophage-depleted mice (Fig. 7B). Infiltration of inflammatory cells is associated with bladder tissue damage and increased bacterial burden (26). As we observed fewer monocytes and eosinophils in macrophage-depleted mice during challenge infection, we investigated whether reduced cell infiltration was associated with less tissue damage. We assessed edema formation by quantifying the area of the lamina propria in post-challenged bladders, depleted of macrophages or not (Fig. 7A). We did not detect a difference in edema formation between nondepleted mice and mice depleted of macrophage before challenge infection (Fig. 7C).

As we observed fewer eosinophils in macrophage-depleted mice during challenge infection, and our previous work demonstrated that type 2 immune response–related cytokines are expressed early in UTI (24), we assessed the polarity of the T cell response to challenge infection (fig. S7, gating strategy). Macrophage depletion did not alter the infiltration of T regulatory cells or T$_H$2 or T$_H$17 T helper subsets (Fig. 7D). However, macrophage depletion did correlate with an increase in the numbers of T$_H$1 T cells, NKT cells, NK cells, and type 1 innate lymphoid cells (ILC1s) (Fig. 7E). In macrophage-depleted mice, T$_H$1 T cells, NKT cells, and NK cells had higher IFN-γ production compared to mock-treated mice (Fig. 7F), suggesting that, in the absence of post-infected macrophages, a more pro-inflammatory, bactericidal response to challenge infection arises in the bladder.

DISCUSSION

Despite numerous studies of macrophage ontogeny and function in many organs, the developmental origin and role of bladder macrophages are largely unknown. Here, we investigated this poorly understood compartment in homeostasis and a highly inflammatory infectious disease, UTI. A single macrophage population of yolk sac and HSC origin seeds the developing bladder; however, the yolk sac macrophage pool is ultimately replaced at some point after birth. After birth, two subsets, MacM and MacL, arise in the tissue, localizing to the muscle and the lamina propria, respectively. These subsets share similar developmental origin, in that they are primarily HSC-derived and, in adulthood, display a very slow turnover by Ly6C$^+$ monocytes in the steady state. Their distinct transcriptomics support the idea that they play different roles in the bladder, at least in the context of infection. The MacM subset is poised to take up bacteria or potentially infected dying host cells, while polarizing toward a more alternatively activated profile during UTI. MacL macrophages express a profile with greater potential for the induction of inflammation and, whether due to direct consequences of this inflammation or potentially due to loss of the urothelium, undergo pronounced cell death during UTI.

In adult animals, steady-state tissue-resident macrophages are a mix of embryonic and adult monocyte-derived macrophages, with the exception of brain microglia (8, 14). The contributions from embryonic macrophages and circulating adult monocytes to the adult bladder macrophage compartment are similar to that of the lung and kidney (7, 11, 77). Although two macrophage subsets reside in the adult bladder, only a single LYVE1$^+$CX$_3$CR1$^+$ macrophage population was identified in embryonic and newborn bladders. As the bladder is fully formed in newborn mice (78), it is unlikely that macrophage subsets arise to meet the needs of a new structure, as is the case for peritubular macrophages in the testis (41). Rather, although all structures are present, embryonic or prenatal bladder tissue demands are likely distinct from postnatal tissue remodeling in very young mice. For example, in the first weeks after birth, bladder macrophages may support urothelial cells undergoing increased proliferation to establish the three layers of urothelium in adult bladders (79). As these adult tissue niches become fully mature, they may provide different growth or survival factors, driving functional macrophage specialization in discrete locations in the tissue.

In the lung, spleen, BM, and liver, a subpopulation of pro-resolving macrophages are present that phagocytize blood-borne cellular material to maintain tissue homeostasis (66). These macrophages express *Mrc1* (encoding for CD206), *CD163*, and *Timd4* (encoding TIM4) (66). MacM macrophages likely represent this subpopulation in the bladder, as they expressed higher levels of genes associated with a pro-resolving phenotype, including the efferocytic receptor TIM4, CD206, and CD163. It is also possible that, similar to muscularis macrophages in the gut, MacM macrophages interact with neurons to control muscle contraction in the bladder and limit neuronal damage during infection (80, 81). By contrast, up-regulated pathways in the MacL subset, in combination with their localization under the urothelium, suggest that, similar to intestinal macrophages, they may regulate T cell responses to bladder microbiota or support urothelial cell integrity (82, 83).

Although it was somewhat unexpected, given that the MacM macrophage subset is located farther from the lumen and urothelium, where infection takes place, we favor the conclusion that MacM macrophages contain more bacteria because they are programmed to do so. This conclusion is supported by the higher expression of genes associated with *complement*, *endocytosis*, and *phagosome* pathways in the MacM subset. It is possible, although challenging to empirically demonstrate, that the MacM subset recognizes dying neutrophils,
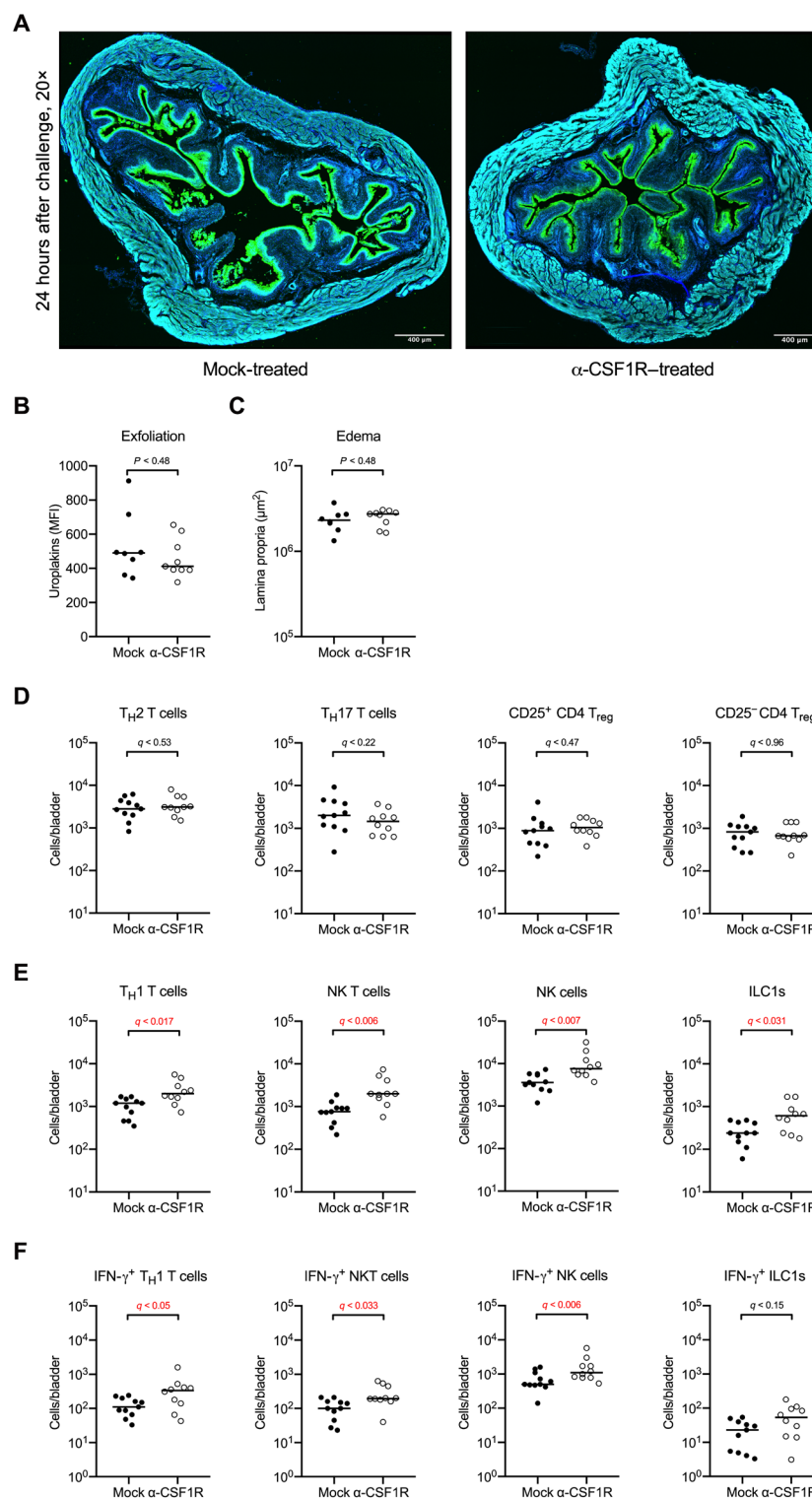
Fig. 7. Depletion of replaced macrophages leads to a type I immune bias. Female C57BL/6 mice were infected according to the scheme shown in Fig. 6A and treated with 800 μg of anti-CSF1R antibody 72 hours before challenge infection with 10^7 CFU of UTI89. (**A**) Representative confocal images of bladders from mice treated with PBS or 800 μg of anti-CSF1R antibody 24 hours after challenge. Uroplakin, green; phalloidin, turquoise; DAPI, blue. (**B**) The graph shows the mean fluorescence intensity of uroplakin expression, quantified from imaging, at 24 hours after challenge. (**C**) The graph shows the area of the lamina propria, quantified from imaging, at 24 hours after challenge. (**D** to **F**) Graphs depict the (D and E) total number of the indicated cell type or (F) the total number of the indicated cell type expressing IFN-γ at 24 hours after challenge infection. Data are pooled from two experiments, $n = 4$ to 6 mice per experiment. Each dot represents one mouse; lines are medians. In (B) to (F), significance was determined using the nonparametric Mann-Whitney test and P values were corrected for multiple testing using the FDR method. All calculated/corrected P values are shown and P values meeting the criteria for statistical significance ($P < 0.05$) are depicted in red.

or even dying MacL macrophages, that have phagocytosed bacteria. We may also consider that, between the subsets, the rate at which bacteria are killed is different, UPEC may survive better in MacM macrophages, MacL macrophages may die after bacterial uptake, the near-luminal location of MacL macrophages may result in their disproportionate sloughing, or even that MacL macrophages break down phagocytosed content better. Additional genetic and knock-out models would be needed to address these possibilities.

Significant numbers of MacL macrophages died in the first hours following infection, reflecting their enriched apoptosis pathway. The reduced numbers of both macrophage subsets in protamine sulfate-treated mice suggest that alterations in the urothelium may affect macrophage survival, although we cannot rule out the fact that protamine sulfate directly kills macrophages. Exfoliation induced by protamine sulfate is not comparable to infection, as protamine sulfate induces a rapid, large increase in trans-urothelial conductance (71), suggesting that it induces major disruptions in the urothelium. Protamine sulfate can also suppress cytokine activity and the inflammatory response in the bladder compared to UPEC infection (84). This severe disruption of the urothelium may lead to inadequate supplies of oxygen, nutrients, or survival factors, all of which would be detrimental to macrophage survival. It is less likely that bacteria induce macrophage death as only a small, and importantly equivalent, proportion of both subsets were infected. Instead, MacL macrophage death may be an important step to initiate immune responses to UTI. In the liver, Kupffer cell death by necroptosis during *Listeria monocytogenes* infection induces recruitment of monocytes, which, in turn, phagocytose bacteria (85). Here, macrophage depletion before challenge infection resulted in decreased infiltration of monocytes, likely due to diminished numbers of these cells in circulation, and fewer eosinophils; however, bacterial burden was also decreased. This suggests that macrophage-mediated immune cell recruitment is not their primary function in the bladder. Infiltration of inflammatory cells is not the only way macrophage cell death regulates infection, however. For instance, pyroptotic macrophages can entrap live bacteria and facilitate their elimination by neutrophils in vivo (86). As MacM macrophages express genes regulating iron metabolism, limiting iron to UPEC would also be a plausible mechanism to control bacterial growth (87).

In the steady state, tissue-resident macrophages can self-maintain locally by proliferation, with minimal input of circulating monocytes (9, 88). By contrast, under inflammatory conditions, resident macrophages are often replaced by monocyte-derived macrophages (85, 88–90). Monocytes will differentiate into self-renewing functional macrophages if the endogenous tissue-resident macrophages are depleted or absent (91, 92). Our results show that UPEC infection induces sufficient inflammation to foster infiltration and differentiation of newly recruited monocytes. It is likely, even, that greater macrophage replacement occurs than we actually measured, as we used a single 4OHT pulse in CCR2^{CreERT2} Rosa26^{tdTomato} mice 24 hours before infection; however, these cells infiltrate infected bladders over several days. These experiments do not rule out a role for local proliferation in the bladder during UTI, but experiments to test this must be able to distinguish infiltrated monocytes that have already differentiated into tissue macrophages from bona fide tissue-resident macrophages when assessing proliferating cells. These data do support, however, the fact that infiltrating monocytes remain in the tissue, integrated into the resident macrophage pool, after tissue resolution.

Recruited monocyte-derived macrophages can behave differently than resident macrophages when activated, such as in the lung. Gamma herpes virus induces alveolar macrophage replacement by "regulatory" monocytes expressing higher levels of Sca-1 and MHC II (93). These post-infected mice have reduced perivascular and peribronchial inflammation and inflammatory cytokines, and fewer eosinophils compared to mock-infected mice when exposed to house dust mite to induce allergic asthma (93). Alveolar macrophages of mice infected with influenza virus are replaced by pro-inflammatory monocyte-derived macrophages. At 30 days PI, influenza-infected mice have more alveolar macrophages and increased production of IL-6 when challenged with *S. pneumoniae* compared to mock-infected mice, leading to fewer deaths (90). Although mechanisms regulating the phenotype of monocyte-derived macrophages are not known, the time of residency in the tissue and the nature of subsequent insults likely influence these cells. The longer that recruited macrophages reside in tissue, the more similar they become to tissue-resident macrophages and no longer provide enhanced protection to subsequent tissue injury (89, 90). In contrast to these studies in the lung, we found that elimination of macrophages, including those recruited during primary infection, led to improved bacterial clearance during secondary challenge, although it is not clear what the long-term consequences on bladder homeostasis might be when a more inflammatory type 1 immune response arises during infection.

Overall, our results demonstrate that two unique subsets of macrophages reside in the bladder. During UTI, these cells respond differently, and a proportion of the population dies. Thus, a first UPEC infection induces replacement of resident macrophage subsets by monocyte-derived cells. When sufficient numbers of MacM macrophages, composed of resident and replaced cells, are depleted, improved bacterial clearance follows, suggesting a major role of this subset in directing the immune response to challenge infection. While these findings greatly improve our understanding of this important immune cell type, much remains to be uncovered, such as the signals and niches that contribute to the establishment of two subsets of bladder-resident macrophages, their roles in the establishment and maintenance of homeostasis, and whether parallel populations and functions exist in human bladder tissue.

MATERIALS AND METHODS
Study design
This study was conducted using a preclinical mouse model and transgenic mouse strains in controlled laboratory experiments to investigate the origin, maintenance, and function of bladder-resident macrophages in homeostasis and bacterial infection. At the onset of this study, our objective was to understand how bladder-resident macrophages negatively affect the development of adaptive immunity to UTI. Having found two resident macrophage subsets in the course of this work, our objectives were to determine whether these subsets have similar origins and homeostatic maintenance and whether they play divergent roles in response to primary or challenge infection. Mice were assigned to groups upon random partition into cages. In all experiments, a minimum of 2 and a maximum of 10 mice (and more typically 3 to 6 mice per experiment) made up an experimental group and all experiments were repeated two to three times. Sample size was based on our previous work and was not changed in the course of the study. In some cases, *n* was limited

by the number of developing embryos available from timed pregnancies. Data collection is detailed below. Data from all repetitions were pooled before any statistical analysis. As determined a priori, all animals with abnormal kidneys (atrophied, enlarged, and white in color) at the time of sacrifice were excluded from all analyses, as we have observed that abnormal kidneys negatively affect resolution of infection. End points were determined before the start of experiments and researchers were not blinded to experimental groups.

Mice and ethical approvals

All animals used in this study had free access to standard laboratory chow and water at all times. We used female C57BL/6J mice 7 to 8 weeks old from Charles River, France. Female CX$_3$CR1$^{GFP/+}$ mice 7 to 8 weeks old were bred in-house. CX$_3$CR1$^{GFP/GFP}$ mice, used to maintain our hemizygous colony, were a gift from F. Chretien (Institut Pasteur). *Cdh5*-CreERT2 Rosa26^{tdTomato} mice were crossed to CX$_3$CR1^{GFP} mice, producing *Cdh5*-CreERT2.Rosa26^{tdTomato}.CX$_3$CR1^{GFP} mice at Centre d'Immunologie de Marseille-Luminy. In *Cdh5*-CreERT2.Rosa26^{tdTomato}.CX$_3$CR1^{GFP} mice, cells expressing the CX$_3$CR1 receptor are constitutively GFP$^+$, and treatment with 4OHT conditionally labels hemogenically active endothelial cells (*42*). We used female and male *Cdh5*-CreERT2.Rosa26^{tdTomato}.CX$_3$CR1^{GFP} mice 8 to 11 weeks old, at E16.5, and newborns. Flt3^{Cre}.Rosa26^{YFP} mice were a gift from E.G.P. (Institut Pasteur). CCR2$^{-/-}$ mice were a gift from M. Lecuit (Institut Pasteur). CCR2creERT2^{BB} mice were a gift from B. Becher (University of Zurich) via S. Amigorena (Institut Curie). CCR2creERT2^{BB} male mice were crossed to Rosa26^{tdTomato} females to obtain CCR2creERT2^{BB}-tdTomato mice at Institut Pasteur. We used female CCR2creERT2^{BB}-tdTomato mice 7 to 8 weeks old. Additional details of the mouse strains used, including JAX and MGI numbers, are listed in table S1. Mice were anesthetized by injection of ketamine (100 mg/kg) and xylazine (5 mg/kg) and euthanized by carbon dioxide inhalation. Experiments were conducted at Institut Pasteur in accordance with approval of protocol number 2016-0010 and dha190501 by the Comité d'éthique en expérimentation animale Paris Centre et Sud (the ethics committee for animal experimentation), in application of the European Directive 2010/63 EU. Experiments with Cdh5-CreERT2 mice were performed in the laboratory of M. Bajenoff, Centre d'Immunologie de Marseille-Luminy, in accordance with national and regional guidelines under protocol number 5-01022012 following review and approval by the local animal ethics committee in Marseille, France.

Reagents and software

Antibodies, reagents, and software used in this study are listed in tables S2, S3, and S4, respectively.

Flow cytometry of bladder tissue and blood

Samples were acquired on a BD LSRFortessa using DIVA software (v8.0.1), and data were analyzed by FlowJo (Treestar) software, including the plugins for downsampling, tSNE, and UMAP (version 10.0). The analysis of bladder and blood was performed as described previously (*23*). Briefly, bladders were dissected and digested in buffer containing Liberase (0.34 U/ml) in phosphate-buffered saline (PBS) at 37°C for 1 hour with manual agitation every 15 min. Digestion was stopped by adding PBS supplemented with 2% fetal bovine serum (FBS) and 0.2 μM EDTA [fluorescence-activated cell sorting (FACS) buffer]. Fc receptors in single-cell suspensions were blocked with anti-mouse CD16/CD32 and stained with antibodies.

Total cell counts were determined by addition of AccuCheck counting beads to a known volume of sample after staining, just before cytometer acquisition. To determine cell populations in the circulation, whole blood was incubated with BD PharmLyse and stained with antibodies (table S2). Total cell counts were determined by the addition of AccuCheck counting beads to 10 μl of whole blood in 1-step Fix/Lyse Solution.

For intracellular staining, single-cell suspensions were resuspended in 1 ml of Golgi stop protein transport inhibitor, diluted (1:1500) in RPMI with 10% FBS, 1% sodium pyruvate, 1× Hepes, 1× nonessential amino acid, 1% penicillin-streptomycin, phorbol 12-myristate 13-acetate (50 ng/ml), and ionomycin (1 μg/ml), and incubated for 4 hours at 37°C. Samples were washed once with FACS buffer, and Fc receptors blocked with anti-mouse CD16/CD32. Samples were stained with antibodies listed in table S2 against surface markers and fixed and permeabilized with 1× fixation and permeabilization buffer and incubated at 4°C for 40 to 50 min protected from light. After incubation, samples were washed two times with 1× permeabilization and wash buffer from the transcription factor buffer kit and stained with antibodies against IFN-γ and the transcriptional factors RORγT, GATA3, T-bet, and FoxP3 (table S2), diluted in 1× permeabilization and wash buffer at 4°C for 40 to 50 min protected from light. Last, samples were washed two times with 1× permeabilization and wash buffer and resuspended in FACS buffer. Total cell counts were determined by addition of counting beads to a known volume of sample after staining, just before cytometer acquisition.

Histological and immunostaining for confocal microscopy

Whole bladders were fixed with 4% paraformaldehyde (PFA) in PBS for 1 hour and subsequently washed with PBS. Samples were then dehydrated in 30% sucrose in PBS for 24 hours. Samples were cut transversally and embedded in optimal cutting temperature compound, frozen, and sectioned at 30 μm. Sections were blocked for 1 hour with blocking buffer [3% bovine serum albumin (BSA) + 0.1% Triton X-100 + donkey serum (1:20) in PBS] and washed three times. Immunostaining was performed using F4/80, LYVE1 antibodies, or polyclonal "asymmetrical unit membrane" antibodies, recognizing uroplakins [gift from X.-R. Wu, NYU School of Medicine, (*76*)] (1:200) in staining buffer (0.5% BSA + 0.1% Triton X-100 in PBS) overnight. Sections were washed and stained with phalloidin (1:350) and secondary antibodies (1:2000) in staining buffer for 4 hours. Last, sections were washed and stained with 4′,6-diamidino-2-phenylindole. Confocal images were acquired on a Leica SP8 confocal microscope. Final image processing was done using Fiji (version 2.0.0-rc-69/1.52p) and Icy software (v1.8.6.0).

Timed pregnancies and in utero tamoxifen administration

Fate mapping of Cdh5-CreERT2 mice was performed as described previously (*42*). Briefly, for reporter recombination in offspring, a single dose of 4OHT supplemented with progesterone (1.2 mg of 4OHT and 0.6 mg of progesterone) was delivered by intraperitoneal injection to pregnant females at E7.5 or E10.5. Progesterone was used to counteract adverse effects of 4OHT on pregnancies. To fate map cells in CCR2creERT2^{BB}-tdTomato mice, a single dose (37.5 μg/g) of 4OHT injection was delivered intraperitoneally.

Shielded BM chimeras

For shielded irradiation, 7- to 8-week-old wild-type female CD45.1 or CD45.2 C57BL6/J mice were anesthetized and dressed in a

lab-made lead diaper, which selectively exposed their tail, legs, torso, and head to irradiation, but protected the lower abdomen, including the bladder. Mice were irradiated with 9 gray from an Xstrahl x-ray generator (250 kV, 12 mA) and reconstituted with ~3×10^7 to 4×10^7 BM cells isolated from congenic (CD45.1) wild-type mice or CD45.2 $CCR2^{-/-}$ mice.

RNA-seq and bioinformatic analyses
Samples were obtained from the whole bladders of naïve and 6-week post-infected female C57BL/6J mice. Using FACS, four separate sorts were performed to generate biological replicates, and each sort was a pool of 10 mouse bladders. Macrophage subsets were FACS-purified into 350 μl of RLT Plus buffer from the RNeasy Micro Kit plus (1:100) β-mercaptoethanol. Total RNA was extracted using the RNeasy Micro Kit following the manufacturer's instructions. Directional libraries were prepared using the Smarter Stranded Total RNA-Seq kit Pico Input Mammalian following the manufacturer's instructions. The quality of libraries was assessed with the DNA-1000 kit on a 2100 Bioanalyzer, and quantification was performed with Quant-It assays on a Qubit 3.0 fluorometer. Clusters were generated for the resulting libraries with Illumina HiSeq SR Cluster Kit v4 reagents. Sequencing was performed with the Illumina HiSeq 2500 system and HiSeq SBS kit v4 reagents. Runs were carried out over 65 cycles, including seven indexing cycles, to obtain 65-bp single-end reads. Sequencing data were processed with Illumina Pipeline software (Casava version 1.9). Reads were cleaned of adapter sequences and low-quality sequences using cutadapt version 1.11. Only sequences of at least 25 nucleotides in length were considered for further analysis, and the five first bases were trimmed following the library manufacturer's instructions. STAR version 2.5.0a (94), with default parameters, was used for alignment on the reference genome (*Mus musculus* GRCm38_87 from Ensembl version 87). Genes were counted using featureCounts version 1.4.6-p3 (95) from Subreads package (parameters: -t exon -g gene_id -s 1). Count data were analyzed using R version 3.4.3 and the Bioconductor package DESeq2 version 1.18.1 (96). The normalization and dispersion estimation were performed with DESeq2 using the default parameters, and statistical tests for differential expression were performed applying the independent filtering algorithm. A generalized linear model was set to test for the differential expression among the four biological conditions. For each pairwise comparison, raw P values were adjusted for multiple testing according to the Benjamini and Hochberg procedure and genes with an adjusted P value lower than 0.05 were considered differentially expressed. Count data were transformed using variance stabilizing transformation to perform samples clustering and PCA plot. The PCA was performed on the variance-stabilized transformed count matrix that was adjusted for the batch/replicate effect using the limma R package version 3.44.3.

To perform pathway analysis, gene lists of DEGs were imported in the Cytoscape software (version 3.7.2), and analyses were performed using the ClueGO application with the Kyoto Encyclopedia of Genes and Genomes as the database. Significant pathways were selected using the threshold criteria $Q < 0.05$; terms > 3 genes; % genes/term > 3; κ 0.4.

Bacterial strains and infection
We used the human UPEC cystitis isolate UTI89 engineered to express the fluorescent proteins RFP or GFP and antibiotic-resistant cassettes to either kanamycin (UPEC-RFP) or ampicillin (UPEC-GFP) to infect animals for flow cytometric and bacterial burden analyses (23). We used the nonfluorescent parental strain UTI89 for confocal imaging experiments and flow cytometric experiments with $CCR2^{CreERT2}$ $Rosa26^{tdTomato}$ mice (97). To allow expression of type 1 pili, necessary for infection (98), bacteria cultures were grown statically in Luria-Bertani broth medium for 18 hours at 37°C in the presence of antibiotics [kanamycin (50 μg/ml) or ampicillin (100 μg/ml)]. Primary and challenge UTI were induced in mice as previously described (23, 99). For challenge infection, urine was collected twice a week, for 4 weeks, to follow the presence of bacteria in the urine. Once there were no UTI89-RFP bacteria in the urine, mice were challenged with UTI89-GFP bacteria and euthanized 24 hours after challenge infection. To calculate CFU, bladders were aseptically removed and homogenized in 1 ml of PBS. Serial dilutions were plated on LB agar plates with antibiotics, as required. For in vitro infections, macrophage subsets were sorted from a pool of 10 bladders of naïve female C57BL/6J 7- to 8-week-old mice using FACS and 2×10^3 cells were incubated with 2×10^4 CFU of UPEC-RFP for 2 hours at 37°C. Cells were acquired on a BD LSR-Fortessa using DIVA software (v8.0.1) and data were analyzed by FlowJo (Treestar) software (version 10.0).

Protamine sulfate administration
Seven- to 8-week-old wild-type female C57BL6/J mice were anesthetized and instilled intravesically with 50 μl of protamine sulfate (50 mg/ml) diluted in PBS and euthanized 5 hours after instillation for analysis.

Immune cell depletion
To produce anti-CSF1R antibody, the hybridoma cell line AFS98 (gift from M. Merad at Icahn School of Medicine at Mount Sinai) (100) was cultured in disposable reactor cell culture flasks for 14 days, and antibodies were purified with disposable PD10 desalting columns. To deplete macrophages, wild-type C57BL/6 mice received intravenous injection of anti-CSF1R antibody (2 mg/ml) diluted in PBS. Animals received two or three intravenous injections, on consecutive days, of anti-CSF1R antibody or PBS. To deplete macrophages with a final concentration of 500 μg of anti-CSF1R, we administered 250 μg per mouse on day 1 and 250 μg per mouse on day 2. To deplete macrophages with a final concentration of 800 μg of anti-CSF1R, we administered 400 μg per mouse on day 1, 200 μg per mouse on day 2, and 200 μg per mouse on day 3 to minimize the impact on circulating monocytes.

Quantification of macrophage subsets, urothelial exfoliation, and tissue edema
To quantify macrophage subsets in bladder tissue, six to seven images were randomly acquired of each of the areas of the muscle and lamina propria per mouse in wild-type C57BL/6 female mice with 40× magnification in an SP8 Leica microscope. Maximum intensity Z-projections were performed, and macrophage subsets were counted using Icy software (v1.8.6.0). To quantify urothelial exfoliation and tissue edema, images from whole bladder cross sections were acquired using 20× magnification in an SP8 Leica microscope. Maximum intensity Z-projections were performed, the urothelium was delimited, and mean fluorescence intensity of uroplakin staining was measured using Fiji (v1.51j) software. To quantify tissue edema, the lamina propria was delimited and the area was measured using Fiji software (v1.51j).

Statistical analysis

Statistical analysis was performed in GraphPad Prism 8 (GraphPad, USA) for Mac OS X applying the nonparametric Wilcoxon test for paired data or the nonparametric Mann-Whitney test for unpaired data in the case of two group comparisons. In the case that more than two groups were being compared or to correct for comparisons made within an entire analysis or experiment, calculated P values were corrected for multiple testing with the false discovery rate (FDR) method (https://jboussier.shinyapps.io/MultipleTesting/) to determine the FDR-adjusted P value. All calculated P values are shown in the figures, and those that met the criteria for statistical significance ($P < 0.05$) are denoted with red text.

SUPPLEMENTARY MATERIALS

Supplementary material for this article is available at http://advances.sciencemag.org/cgi/content/full/6/48/eabc5739/DC1

View/request a protocol for this paper from *Bio-protocol*.

REFERENCES AND NOTES

1. T. A. Wynn, A. Chawla, J. W. Pollard, Macrophage biology in development, homeostasis and disease. *Nature* **496**, 445–455 (2013).
2. S. Epelman, K. J. Lavine, G. J. Randolph, Origin and functions of tissue macrophages. *Immunity* **41**, 21–35 (2014).
3. I. Amit, D. R. Winter, S. Jung, The role of the local environment and epigenetics in shaping macrophage identity and their effect on tissue homeostasis. *Nat. Immunol.* **17**, 18–25 (2016).
4. M. A. Ingersoll, M. L. Albert, From infection to immunotherapy: Host immune responses to bacteria at the bladder mucosa. *Mucosal Immunol.* **6**, 1041–1053 (2013).
5. L. Lacerda Mariano, M. A. Ingersoll, Bladder resident macrophages: Mucosal sentinels. *Cell. Immunol.* **330**, 136–141 (2018).
6. G. Hoeffel, J. Chen, Y. Lavin, D. Low, F. F. Almeida, P. See, A. E. Beaudin, J. Lum, I. Low, E. C. Forsberg, M. Poidinger, F. Zolezzi, A. Larbi, L. G. Ng, J. K. Y. Chan, M. Greter, B. Becher, I. M. Samokhvalov, M. Merad, F. Ginhoux, C-Myb⁺ erythro-myeloid progenitor-derived fetal monocytes give rise to adult tissue-resident macrophages. *Immunity* **42**, 665–678 (2015).
7. C. Schulz, E. G. Perdiguero, L. Chorro, H. Szabo-Rogers, N. Cagnard, K. Kierdorf, M. Prinz, B. Wu, S. E. W. Jacobsen, J. W. Pollard, J. Frampton, K. J. Liu, F. Geissmann, A lineage of myeloid cells independent of Myb and hematopoietic stem cells. *Science* **336**, 86–90 (2012).
8. F. Ginhoux, M. Greter, M. Leboeuf, S. Nandi, P. See, S. Gokhan, M. F. Mehler, S. J. Conway, L. G. Ng, E. Richard Stanley, I. M. Samokhvalov, M. Merad, Fate mapping analysis reveals that adult microglia derive from primitive macrophages. *Science* **330**, 841–845 (2010).
9. D. Hashimoto, A. Chow, C. Noizat, P. Teo, M. B. Beasley, M. Leboeuf, C. D. Becker, P. See, J. Price, D. Lucas, M. Greter, A. Mortha, S. W. Boyer, E. Camilla Forsberg, M. Tanaka, N. van Rooijen, A. García-Sastre, E. Richard Stanley, F. Ginhoux, P. S. Frenette, M. Merad, Tissue-resident macrophages self-maintain locally throughout adult life with minimal contribution from circulating monocytes. *Immunity* **38**, 792–804 (2013).
10. S. Yona, K.-W. Kim, Y. Wolf, A. Mildner, D. Varol, M. Breker, D. Strauss-Ayali, S. Viukov, M. Guilliams, A. Misharin, D. A. Hume, H. Perlman, B. Malissen, E. Zelzer, S. Jung, Fate mapping reveals origins and dynamics of monocytes and tissue macrophages under homeostasis. *Immunity* **38**, 79–91 (2013).
11. S. Epelman, K. J. Lavine, A. E. Beaudin, D. K. Sojka, J. A. Carrero, B. Calderon, T. Brija, E. L. Gautier, S. Ivanov, A. T. Satpathy, J. D. Schilling, R. Schwendener, I. Sergin, B. Razani, E. Camilla Forsberg, W. M. Yokoyama, E. R. Unanue, M. Colonna, G. J. Randolph, D. L. Mann, Embryonic and adult-derived resident cardiac macrophages are maintained through distinct mechanisms at steady state and during inflammation. *Immunity* **40**, 91–104 (2014).
12. M. Guilliams, I. De Kleer, S. Henri, S. Post, L. Vanhoutte, S. De Prijck, K. Deswarte, B. Malissen, H. Hammad, B. N. Lambrecht, Alveolar macrophages develop from fetal monocytes that differentiate into long-lived cells in the first week of life via GM-CSF. *J. Exp. Med.* **210**, 1977–1992 (2013).
13. F. Ginhoux, M. Guilliams, Tissue-resident macrophage ontogeny and homeostasis. *Immunity* **44**, 439–449 (2016).
14. E. Gomez Perdiguero, K. Klapproth, C. Schulz, K. Busch, E. Azzoni, L. Crozet, H. Garner, C. Trouillet, M. F. de Bruijn, F. Geissmann, H.-R. Rodewald, Tissue-resident macrophages originate from yolk-sac-derived erythro-myeloid progenitors. *Nature* **518**, 547–551 (2015).
15. G. Hoeffel, F. Ginhoux, Fetal monocytes and the origins of tissue-resident macrophages. *Cell. Immunol.* **330**, 5–15 (2018).
16. C. C. Bain, A. Bravo-Blas, C. L. Scott, E. G. Perdiguero, F. Geissmann, S. Henri, B. Malissen, L. C. Osborne, D. Artis, A. M. Mowat, Constant replenishment from circulating monocytes maintains the macrophage pool in the intestine of adult mice. *Nat. Immunol.* **15**, 929–937 (2014).
17. S. De Schepper, S. Verheijden, J. Aguilera-Lizarraga, M. F. Viola, W. Boesmans, N. Stakenborg, I. Voytyuk, I. Schmidt, B. Boeckx, I. D. de Casterlé, V. Baekelandt, E. G. Dominguez, M. Mack, I. Depoortere, B. De Strooper, B. Sprangers, U. Himmelreich, S. Soenen, M. Guilliams, P. V. Berghe, E. Jones, D. Lambrechts, G. Boeckxstaens, Self-maintaining gut macrophages are essential for intestinal homeostasis. *Cell* **176**, 676 (2019).
18. S. A. Dick, J. A. Macklin, S. Nejat, A. Momen, X. Clemente-Casares, M. G. Althagafi, J. Chen, C. Kantores, S. Hosseinzadeh, L. Aronoff, A. Wong, R. Zaman, I. Barbu, R. Besla, K. J. Lavine, B. Razani, F. Ginhoux, M. Husain, M. I. Cybulsky, C. S. Robbins, S. Epelman, Self-renewing resident cardiac macrophages limit adverse remodeling following myocardial infarction. *Nat. Immunol.* **20**, 29–39 (2019).
19. Y. Lavin, D. Winter, R. Blecher-Gonen, E. David, H. Keren-Shaul, M. Merad, S. Jung, I. Amit, Tissue-resident macrophage enhancer landscapes are shaped by the local microenvironment. *Cell* **159**, 1312–1326 (2014).
20. D. Gosselin, V. M. Link, C. E. Romanoski, G. J. Fonseca, D. Z. Eichenfield, N. J. Spann, J. D. Stender, H. B. Chun, H. Garner, F. Geissmann, C. K. Glass, Environment drives selection and function of enhancers controlling tissue-specific macrophage identities. *Cell* **159**, 1327–1340 (2014).
21. I. Gabanyi, P. A. Muller, L. Feighery, T. Y. Oliveira, F. A. Costa-Pinto, D. Mucida, Neuro-immune interactions drive tissue programming in intestinal macrophages. *Cell* **164**, 378–391 (2016).
22. B. Foxman, Epidemiology of urinary tract infections: Incidence, morbidity, and economic costs. *Am. J. Med.* **113** (Suppl. 1A), 5S–13S (2002).
23. G. Mora-Bau, A. M. Platt, N. van Rooijen, G. J. Randolph, M. L. Albert, M. A. Ingersoll, Macrophages subvert adaptive immunity to urinary tract infection. *PLOS Pathog.* **11**, e1005044 (2015).
24. A. Zychlinsky Scharff, M. Rousseau, L. L. Mariano, T. Canton, C. R. Consiglio, M. L. Albert, M. Fontes, D. Duffy, M. A. Ingersoll, Sex differences in IL-17 contribute to chronicity in male versus female urinary tract infection. *JCI Insight* **5**, e122998 (2019).
25. M. Haraoka, L. Hang, B. Frendéus, G. Godaly, M. Burdick, R. Strieter, C. Svanborg, Neutrophil recruitment and resistance to urinary tract infection. *J. Infect. Dis.* **180**, 1220–1229 (1999).
26. M. A. Ingersoll, K. A. Kline, H. V. Nielsen, S. J. Hultgren, G-CSF induction early in uropathogenic *Escherichia coli* infection of the urinary tract modulates host immunity. *Cell. Microbiol.* **10**, 2568–2578 (2008).
27. L. Hang, M. Haraoka, W. W. Agace, H. Leffler, M. Burdick, R. Strieter, C. Svanborg, Macrophage inflammatory protein-2 is required for neutrophil passage across the epithelial barrier of the infected urinary tract. *J. Immunol.* **162**, 3037–3044 (1999).
28. R. D. Shahin, I. Engberg, L. Hagberg, C. Svanborg Edén, Neutrophil recruitment and bacterial clearance correlated with LPS responsiveness in local gram-negative infection. *J. Immunol.* **138**, 3475–3480 (1987).
29. T. L. Denning, Y.-c. Wang, S. R. Patel, I. Williams, B. Pulendran, Lamina propria macrophages and dendritic cells differentially induce regulatory and interleukin 17-producing T cell responses. *Nat. Immunol.* **8**, 1086–1094 (2007).
30. C. Panea, A. M. Farkas, Y. Goto, S. Abdollahi-Roodsaz, C. Lee, B. Koscsó, K. Gowda, T. M. Hohl, M. Bogunovic, I. I. Ivanov, Intestinal monocyte-derived macrophages control commensal-specific Th17 responses. *Cell Rep.* **12**, 1314–1324 (2015).
31. N. P. Goplen, S. Huang, B. Zhu, I. S. Cheon, Y. M. Son, Z. Wang, C. Li, Q. Dai, L. Jiang, J. Sun, Tissue-resident macrophages limit pulmonary CD8 resident memory T cell establishment. *Front. Immunol.* **10**, 2332 (2019).
32. T. Bergsbaken, M. J. Bevan, P. J. Fink, Local inflammatory cues regulate differentiation and persistence of CD8⁺ tissue-resident memory T cells. *Cell Rep.* **19**, 114–124 (2017).
33. M. D. Taylor, A. Harris, M. G. Nair, R. M. Maizels, J. E. Allen, F4/80⁺ alternatively activated macrophages control CD4⁺ T cell hyporesponsiveness at sites peripheral to filarial infection. *J. Immunol.* **176**, 6918–6927 (2006).
34. J. M. Austyn, S. Gordon, F4/80, a monoclonal antibody directed specifically against the mouse macrophage. *Eur. J. Immunol.* **11**, 805–815 (1981).
35. E. L. Gautier, T. Shay, J. Miller, M. Greter, C. Jakubzick, S. Ivanov, J. Helft, A. Chow, K. G. Elpek, S. Gordonov, A. R. Mazloom, A. Ma'ayan, W.-J. Chua, T. H. Hansen, S. J. Turley, M. Merad, G. J. Randolph; Immunological Genome Consortium, Gene-expression profiles and transcriptional regulatory pathways that underlie the identity and diversity of mouse tissue macrophages. *Nat. Immunol.* **13**, 1118–1128 (2012).
36. S. Jung, J. Aliberti, P. Graemmel, M. J. Sunshine, G. W. Kreutzberg, A. Sher, D. R. Littman, Analysis of fractalkine receptor CX₃CR1 function by targeted deletion and green fluorescent protein reporter gene insertion. *Mol. Cell. Biol.* **20**, 4106–4114 (2000).

37. O. Medina-Contreras, D. Geem, O. Laur, I. R. Williams, S. A. Lira, A. Nusrat, C. A. Parkos, T. L. Denning, CX3CR1 regulates intestinal macrophage homeostasis, bacterial translocation, and colitogenic Th17 responses in mice. *J. Clin. Invest.* **121**, 4787–4795 (2011).

38. Z. Tang, Y. Gan, Q. Liu, J.-X. Yin, Q. Liu, J. Shi, F.-D. Shi, CX3CR1 deficiency suppresses activation and neurotoxicity of microglia/macrophage in experimental ischemic stroke. *J. Neuroinflammation* **11**, 26 (2014).

39. S. Chakarov, H. Y. Lim, L. Tan, S. Y. Lim, P. See, J. Lum, X.-M. Zhang, S. Foo, S. Nakamizo, K. Duan, W. T. Kong, R. Gentek, A. Balachander, D. Carbajo, C. Bleriot, M. Malleret, J. K. C. Tam, S. Baig, M. Shabeer, S.-A. E. S. Toh, A. Schlitzer, A. Larbi, T. Marichal, B. Malissen, J. Chen, M. Poidinger, K. Kabashima, M. Bajenoff, L. G. Ng, V. Angeli, F. Ginhoux, Two distinct interstitial macrophage populations coexist across tissues in specific subtissular niches. *Science* **363**, eaau0964 (2019).

40. K. Molawi, Y. Wolf, P. K. Kandalla, J. Favret, N. Hagemeyer, K. Frenzel, A. R. Pinto, K. Klapproth, S. Henri, B. Malissen, H.-R. Rodewald, N. A. Rosenthal, M. Bajenoff, M. Prinz, S. Jung, M. H. Sieweke, Progressive replacement of embryo-derived cardiac macrophages with age. *J. Exp. Med.* **211**, 2151–2158 (2014).

41. N. Mossadegh-Keller, R. Gentek, G. Gimenez, S. Bigot, S. Mailfert, M. H. Sieweke, Developmental origin and maintenance of distinct testicular macrophage populations. *J. Exp. Med.* **214**, 2829–2841 (2017).

42. R. Gentek, C. Ghigo, G. Hoeffel, M. J. Bulle, R. Msallam, G. Gautier, P. Launay, J. Chen, F. Ginhoux, M. Bajénoff, Hemogenic endothelial fate mapping reveals dual developmental origin of mast cells. *Immunity* **48**, 1160–1171.e5 (2018).

43. S. W. Boyer, A. V. Schroeder, S. Smith-Berdan, E. C. Forsberg, All hematopoietic cells develop from hematopoietic stem cells through Flk2/Flt3-positive progenitor cells. *Cell Stem Cell* **9**, 64–73 (2011).

44. N. V. Serbina, E. G. Pamer, Monocyte emigration from bone marrow during bacterial infection requires signals mediated by chemokine receptor CCR2. *Nat. Immunol.* **7**, 311–317 (2006).

45. M. Baratin, L. Simon, A. Jorquera, C. Ghigo, D. Dembele, J. Nowak, R. Gentek, S. Wienert, F. Klauschen, B. Malissen, M. Dalod, M. Bajénoff, T cell zone resident macrophages silently dispose of apoptotic cells in the lymph node. *Immunity* **47**, 349–362.e5 (2017).

46. C. C. Bain, C. A. Hawley, H. Garner, C. L. Scott, A. Schridde, N. J. Steers, M. Mack, A. Joshi, M. Guilliams, A. M. Mowat, F. Geissmann, S. J. Jenkins, Long-lived self-renewing bone marrow-derived macrophages displace embryo-derived cells to inhabit adult serous cavities. *Nat. Commun.* **7**, ncomms11852 (2016).

47. A. Waterstrat, Y. Liang, C. F. Swiderski, B. J. Shelton, G. Van Zant, Congenic interval of CD45/Ly-5 congenic mice contains multiple genes that may influence hematopoietic stem cell engraftment. *Blood* **115**, 408–417 (2010).

48. F. E. Mercier, D. B. Sykes, D. T. Scadden, Single targeted exon mutation creates a true congenic mouse for competitive hematopoietic stem cell transplantation: The C57BL/6-CD45.1^STEM mouse. *Stem Cell Reports* **6**, 985–992 (2016).

49. X. Han, R. Wang, Y. Zhou, L. Fei, H. Sun, S. Lai, A. Saadatpour, Z. Zhou, H. Chen, F. Ye, D. Huang, Y. Xu, W. Huang, M. Jiang, X. Jiang, J. Mao, Y. Chen, C. Lu, J. Xie, Q. Fang, Y. Wang, R. Yue, T. Li, H. Huang, S. H. Orkin, G.-C. Yuan, M. Chen, G. Guo, Mapping the Mouse Cell Atlas by Microwell-Seq. *Cell* **172**, 1091–1107.e17 (2018).

50. K. D. Nguyen, Y. Qiu, X. Cui, Y. P. S. Goh, J. Mwangi, T. David, L. Mukundan, F. Brombacher, R. M. Locksley, A. Chawla, Alternatively activated macrophages produce catecholamines to sustain adaptive thermogenesis. *Nature* **480**, 104–108 (2011).

51. G. Raes, R. Van den Bergh, P. De Baetselier, G. H. Ghassabeh, C. Scotton, M. Locati, A. Mantovani, S. Sozzani, Arginase-1 and Ym1 are markers for murine, but not human, alternatively activated myeloid cells. *J. Immunol.* **174**, 6561; author reply 6561–6561; author reply 6562 (2005).

52. D. T. Ploeger, N. A. Hosper, M. Schipper, J. A. Koerts, S. de Rond, R. A. Bank, Cell plasticity in wound healing: Paracrine factors of M1/M2 polarized macrophages influence the phenotypical state of dermal fibroblasts. *Cell Commun. Signal* **11**, 29 (2013).

53. D. Voehringer, N. van Rooijen, R. M. Locksley, Eosinophils develop in distinct stages and are recruited to peripheral sites by alternatively activated macrophages. *J. Leukoc. Biol.* **81**, 1434–1444 (2007).

54. M. Nairz, I. Theurl, F. K. Swirski, G. Weiss, "Pumping iron"—How macrophages handle iron at the systemic, microenvironmental, and cellular levels. *Pflugers Arch.* **469**, 397–418 (2017).

55. A. Schridde, C. C. Bain, J. U. Mayer, J. Montgomery, E. Pollet, B. Denecke, S. W. F. Milling, S. J. Jenkins, M. Dalod, S. Henri, B. Malissen, O. Pabst, A. M. Mowat, Tissue-specific differentiation of colonic macrophages requires TGFβ receptor-mediated signaling. *Mucosal Immunol.* **10**, 1387–1399 (2017).

56. C. C. Bain, A. Schridde, Origin, differentiation, and function of intestinal macrophages. *Front. Immunol.* **9**, 2733 (2018).

57. C. Agostini, L. Trentin, A. Perin, M. Facco, M. Siviero, F. Piazza, U. Basso, F. Adami, R. Zambello, G. Semenzato, Regulation of alveolar macrophage-T cell interactions during Th1-type sarcoid inflammatory process. *Am. J. Physiol.* **277**, L240–L250 (1999).

58. S. Matsumura, B. Wang, N. Kawashima, S. Braunstein, M. Badura, T. O. Cameron, J. S. Babb, R. J. Schneider, S. C. Formenti, M. L. Dustin, S. Demaria, Radiation-induced CXCL16 release by breast cancer cells attracts effector T cells. *J. Immunol.* **181**, 3099–3107 (2008).

59. X. Jiang, T. Shimaoka, S. Kojo, M. Harada, H. Watarai, H. Wakao, N. Ohkohchi, S. Yonehara, M. Taniguchi, K.-i. Seino, Cutting edge: Critical role of CXCL16/CXCR6 in NKT cell trafficking in allograft tolerance. *J. Immunol.* **175**, 2051–2055 (2005).

60. J. R. Jackson, B. Bolognese, C. A. Mangar, W. C. Hubbard, L. A. Marshall, J. D. Winkler, The role of platelet activating factor and other lipid mediators in inflammatory angiogenesis. *Biochim. Biophys. Acta* **1392**, 145–152 (1998).

61. T. Shimizu, Lipid mediators in health and disease: Enzymes and receptors as therapeutic targets for the regulation of immunity and inflammation. *Annu. Rev. Pharmacol. Toxicol.* **49**, 123–150 (2009).

62. B. Beutler, Tlr4: Central component of the sole mammalian LPS sensor. *Curr. Opin. Immunol.* **12**, 20–26 (2000).

63. D. Montoya, D. Cruz, R. M. B. Teles, D. J. Lee, M. T. Ochoa, S. R. Krutzik, R. Chun, M. Schenk, X. Zhang, B. G. Ferguson, A. E. Burdick, E. N. Sarno, T. H. Rea, M. Hewison, J. S. Adams, G. Cheng, R. L. Modlin, Divergence of macrophage phagocytic and antimicrobial programs in leprosy. *Cell Host Microbe* **6**, 343–353 (2009).

64. J. Tang, B. Zhou, M. J. Scott, L. Chen, D. Lai, E. K. Fan, Y. Li, Q. Wu, T. R. Billiar, M. A. Wilson, P. Wang, J. Fan, EGFR signaling augments TLR4 cell surface expression and function in macrophages via regulation of Rab5a activation. *Protein Cell* **11**, 144–149 (2020).

65. N. Sukhbaatar, T. Weichhart, Iron regulation: Macrophages in control. *Pharmaceuticals (Basel)* **11**, 137 (2018).

66. N. A-Gonzalez, J. A. Quintana, S. García-Silva, M. Mazariegos, A. González de la Aleja, J. A. Nicolás-Ávila, W. Walter, J. M. Adrover, G. Crainiciuc, V. K. Kuchroo, C. V. Rothlin, H. Peinado, A. Castrillo, M. Ricote, A. Hidalgo, Phagocytosis imprints heterogeneity in tissue-resident macrophages. *J. Exp. Med.* **214**, 1281–1296 (2017).

67. S. Gordon, F. O. Martinez, Alternative activation of macrophages: Mechanism and functions. *Immunity* **32**, 593–604 (2010).

68. A. M. V. Murthy, M.-D. Phan, K. M. Peters, N. T. K. Nhu, R. A. Welch, G. C. Ulett, M. A. Schembri, M. J. Sweet, Regulation of hemolysin in uropathogenic *Escherichia coli* fine-tunes killing of human macrophages. *Virulence* **9**, 967–980 (2018).

69. K. Schaale, K. M. Peters, A. M. Murthy, A. K. Fritzsche, M.-D. Phan, M. Totsika, A. A. B. Robertson, K. B. Nichols, M. A. Cooper, K. J. Stacey, G. C. Ulett, K. Schroder, M. A. Schembri, M. J. Sweet, Strain- and host species-specific inflammasome activation, IL-1β release, and cell death in macrophages infected with uropathogenic *Escherichia coli*. *Mucosal Immunol.* **9**, 124–136 (2016).

70. M. A. Mulvey, Y. S. Lopez-Boado, C. L. Wilson, R. Roth, W. C. Parks, J. Heuser, S. J. Hultgren, Induction and evasion of host defenses by type 1-piliated uropathogenic *Escherichia coli*. *Science* **282**, 1494–1497 (1998).

71. C. J. Tzan, J. Berg, S. A. Lewis, Effect of protamine sulfate on the permeability properties of the mammalian urinary bladder. *J. Membr. Biol.* **133**, 227–242 (1993).

72. I. U. Mysorekar, S. J. Hultgren, Mechanisms of uropathogenic *Escherichia coli* persistence and eradication from the urinary tract. *Proc. Natl. Acad. Sci. U.S.A.* **103**, 14170–14175 (2006).

73. A. L. Croxford, M. Lanzinger, F. J. Hartmann, B. Schreiner, F. Mair, P. Pelczar, B. E. Clausen, S. Jung, M. Greter, B. Becher, The cytokine GM-CSF drives the inflammatory signature of CCR2+ monocytes and licenses autoimmunity. *Immunity* **43**, 502–514 (2015).

74. M. Gross-Vered, S. Trzebanski, A. Shemer, B. Bernshtein, C. Curato, G. Stelzer, T.-M. Salame, E. David, S. Boura-Halfon, L. Chappell-Maor, D. Leshkowitz, S. Jung, Defining murine monocyte differentiation into colonic and ileal macrophages. *eLife* **9**, e49998 (2020).

75. G. G. Anderson, J. J. Palermo, J. D. Schilling, R. Roth, J. Heuser, S. J. Hultgren, Intracellular bacterial biofilm-like pods in urinary tract infections. *Science* **301**, 105–107 (2003).

76. X. R. Wu, M. Manabe, J. Yu, T. T. Sun, Large scale purification and immunolocalization of bovine uroplakins I, II, and III. Molecular markers of urothelial differentiation. *J. Biol. Chem.* **265**, 19170–19179 (1990).

77. S. Ide, Y. Yahara, Y. Kobayashi, S. A. Strausser, K. Ide, A. Watwe, S. Xu-Vanpala, J. R. Privratsky, S. D. Crowley, M. L. Shinohara, B. A. Alman, T. Souma, Yolk-sac-derived macrophages progressively expand in the mouse kidney with age. *eLife* **9**, e51756 (2020).

78. S. P. Jost, Cell cycle of normal bladder urothelium in developing and adult mice. *Virchows Arch. B Cell Pathol. Incl. Mol. Pathol.* **57**, 27–36 (1989).

79. S. M. Cohen, T. Cano, T. Sakata, S. L. Johansson, Ultrastructural characteristics of the fetal and neonatal rat urinary bladder. *Scanning Microsc.* **2**, 2091–2104 (1988).

80. P. A. Muller, B. Koscsó, G. M. Rajani, K. Stevanovic, M.-L. Berres, D. Hashimoto, A. Mortha, M. Leboeuf, X.-M. Li, D. Mucida, E. R. Stanley, S. Dahan, K. G. Margolis, M. D. Gershon, M. Merad, M. Bogunovic, Crosstalk between muscularis macrophages and enteric neurons regulates gastrointestinal motility. *Cell* **158**, 300–313 (2014).

81. F. Matheis, P. A. Muller, C. L. Graves, I. Gabanyi, Z. J. Kerner, D. Costa-Borges, T. Ahrends, P. Rosenstiel, D. Mucida, Adrenergic signaling in muscularis macrophages limits infection-induced neuronal loss. *Cell* **180**, 64–78.e16 (2020).

82. T. L. Morhardt, A. Hayashi, T. Ochi, M. Quirós, S. Kitamoto, H. Nagao-Kitamoto, P. Kuffa, K. Atarashi, K. Honda, J. Y. Kao, A. Nusrat, N. Kamada, IL-10 produced by macrophages regulates epithelial integrity in the small intestine. *Sci. Rep.* **9**, 1223 (2019).

83. N. A. Scott, A. Andrusaite, P. Andersen, M. Lawson, C. Alcon-Giner, C. Leclaire, S. Caim, G. Le Gall, T. Shaw, J. P. R. Connolly, A. J. Roe, H. Wessel, A. Bravo-Blas, C. A. Thomson, V. Kästele, P. Wang, D. A. Peterson, A. Bancroft, X. Li, R. Grencis, A. M. Mowat, L. J. Hall, M. A. Travis, S. W. F. Milling, E. R. Mann, Antibiotics induce sustained dysregulation of intestinal T cell immunity by perturbing macrophage homeostasis. *Sci. Transl. Med.* **10**, eaao4755 (2018).

84. K. M. Stemler, L. W. Crock, H. H. Lai, J. C. Mills, R. W. Gereau, I. U. Mysorekar, Protamine sulfate induced bladder injury protects from distention induced bladder pain. *J. Urol.* **189**, 343–351 (2013).

85. C. Bleriot, T. Dupuis, G. Jouvion, G. Eberl, O. Disson, M. Lecuit, Liver-resident macrophage necroptosis orchestrates type 1 microbicidal inflammation and type-2-mediated tissue repair during bacterial infection. *Immunity* **42**, 145–158 (2015).

86. I. Jorgensen, Y. Zhang, B. A. Krantz, E. A. Miao, Pyroptosis triggers pore-induced intracellular traps (PITs) that capture bacteria and lead to their clearance by efferocytosis. *J. Exp. Med.* **213**, 2113–2128 (2016).

87. A. E. Robinson, J. R. Heffernan, J. P. Henderson, The iron hand of uropathogenic *Escherichia coli*: The role of transition metal control in virulence. *Future Microbiol.* **13**, 745–756 (2018).

88. M. Merad, M. G. Manz, H. Karsunky, A. Wagers, W. Peters, I. Charo, I. L. Weissman, J. G. Cyster, E. G. Engleman, Langerhans cells renew in the skin throughout life under steady-state conditions. *Nat. Immunol.* **3**, 1135–1141 (2002).

89. A. V. Misharin, L. Morales-Nebreda, P. A. Reyfman, C. M. Cuda, J. M. Walter, A. C. McQuattie-Pimentel, C.-I. Chen, K. R. Anekalla, N. Joshi, K. J. N. Williams, H. Abdala-Valencia, T. J. Yacoub, M. Chi, S. Chiu, F. J. Gonzalez-Gonzalez, K. Gates, A. P. Lam, T. T. Nicholson, P. J. Homan, S. Soberanes, S. Dominguez, V. K. Morgan, R. Saber, A. Shaffer, M. Hinchcliff, S. A. Marshall, A. Bharat, S. Berdnikovs, S. M. Bhorade, E. T. Bartom, R. I. Morimoto, W. E. Balch, J. I. Sznajder, N. S. Chandel, G. M. Mutlu, M. Jain, C. J. Gottardi, B. D. Singer, K. M. Ridge, N. Bagheri, A. Shilatifard, G. R. S. Budinger, H. Perlman, Monocyte-derived alveolar macrophages drive lung fibrosis and persist in the lung over the life span. *J. Exp. Med.* **214**, 2387–2404 (2017).

90. H. Aegerter, J. Kulikauskaite, S. Crotta, H. Patel, G. Kelly, E. M. Hessel, M. Mack, S. Beinke, A. Wack, Influenza-induced monocyte-derived alveolar macrophages confer prolonged antibacterial protection. *Nat. Immunol.* **21**, 145–157 (2020).

91. C. L. Scott, F. Zheng, P. De Baetselier, L. Martens, Y. Saeys, S. De Prijck, C. L. Scott, S. Schoonooghe, G. Raes, N. Devoogdt, B. N. Lambrecht, A. Beschin, M. Guilliams, Bone marrow-derived monocytes give rise to self-renewing and fully differentiated Kupffer cells. *Nat. Commun.* **7**, 10321 (2016).

92. L. van de Laar, W. Saelens, S. De Prijck, L. Martens, C. L. Scott, G. Van Isterdael, E. Hoffmann, R. Beyaert, Y. Saeys, B. N. Lambrecht, M. Guilliams, Yolk sac macrophages, fetal liver, and adult monocytes can colonize an empty niche and develop into functional tissue-resident macrophages. *Immunity* **44**, 755–768 (2016).

93. B. Machiels, M. Dourcy, X. Xiao, J. Javaux, C. Mesnil, C. Sabatel, D. Desmecht, F. Lallemand, P. Martinive, H. Hammad, M. Guilliams, B. Dewals, A. Vanderplasschen, B. N. Lambrecht, F. Bureau, L. Gillet, A gammaherpesvirus provides protection against allergic asthma by inducing the replacement of resident alveolar macrophages with regulatory monocytes. *Nat. Immunol.* **18**, 1310–1320 (2017).

94. A. Dobin, C. A. Davis, F. Schlesinger, J. Drenkow, C. Zaleski, S. Jha, P. Batut, M. Chaisson, T. R. Gingeras, STAR: Ultrafast universal RNA-seq aligner. *Bioinformatics* **29**, 15–21 (2013).

95. Y. Liao, G. K. Smyth, W. Shi, featureCounts: An efficient general purpose program for assigning sequence reads to genomic features. *Bioinformatics* **30**, 923–930 (2014).

96. M. I. Love, W. Huber, S. Anders, Moderated estimation of fold change and dispersion for RNA-seq data with DESeq2. *Genome Biol.* **15**, 550 (2014).

97. M. A. Mulvey, J. D. Schilling, S. J. Hultgren, Establishment of a persistent *Escherichia coli* reservoir during the acute phase of a bladder infection. *Infect. Immun.* **69**, 4572–4579 (2001).

98. S. J. Hultgren, W. R. Schwan, A. J. Schaeffer, J. L. Duncan, Regulation of production of type 1 pili among urinary tract isolates of *Escherichia coli*. *Infect. Immun.* **54**, 613–620 (1986).

99. A. Zychlinsky Scharff, M. L. Albert, M. A. Ingersoll, Urinary tract infection in a small animal model: Transurethral catheterization of male and female mice. *J. Vis. Exp.* , 54432 (2017).

100. D. Hashimoto, A. Chow, M. Greter, Y. Saenger, W.-H. Kwan, M. Leboeuf, F. Ginhoux, J. C. Ochando, Y. Kunisaki, N. van Rooijen, C. Liu, T. Teshima, P. S. Heeger, E. R. Stanley, P. S. Frenette, M. Merad, Pretransplant CSF-1 therapy expands recipient macrophages and ameliorates GVHD after allogeneic hematopoietic cell transplantation. *J. Exp. Med.* **208**, 1069–1082 (2011).

Citation: L. Lacerda Mariano, M. Rousseau, H. Varet, R. Legendre, R. Gentek, J. Saenz Coronilla, M. Bajenoff, E. Gomez Perdiguero, M. A. Ingersoll, Functionally distinct resident macrophage subsets differentially shape responses to infection in the bladder. *Sci. Adv.* **6**, eabc5739 (2020).

Science Advances

Functionally distinct resident macrophage subsets differentially shape responses to infection in the bladder

Livia Lacerda Mariano, Matthieu Rousseau, Hugo Varet, Rachel Legendre, Rebecca Gentek, Javier Saenz Coronilla, Marc Bajenoff, Elisa Gomez Perdiguero and Molly A. Ingersoll

ARTICLE TOOLS	http://advances.sciencemag.org/content/6/48/eabc5739
SUPPLEMENTARY MATERIALS	http://advances.sciencemag.org/content/suppl/2020/11/19/6.48.eabc5739.DC1
REFERENCES	This article cites 99 articles, 24 of which you can access for free http://advances.sciencemag.org/content/6/48/eabc5739#BIBL
PERMISSIONS	http://www.sciencemag.org/help/reprints-and-permissions

Use of this article is subject to the Terms of Service